NASA/TP–2020-220562

Re-Computation of Numerical Results Contained in NACA Report No. 685

Boyd Perry, III
Langley Research Center, Hampton, Virginia

February 2020

NASA STI Program . . . in Profile

Since its founding, NASA has been dedicated to the advancement of aeronautics and space science. The NASA scientific and technical information (STI) program plays a key part in helping NASA maintain this important role.

The NASA STI program operates under the auspices of the Agency Chief Information Officer. It collects, organizes, provides for archiving, and disseminates NASA's STI. The NASA STI program provides access to the NTRS Registered and its public interface, the NASA Technical Reports Server, thus providing one of the largest collections of aeronautical and space science STI in the world. Results are published in both non-NASA channels and by NASA in the NASA STI Report Series, which includes the following report types:

- TECHNICAL PUBLICATION. Reports of completed research or a major significant phase of research that present the results of NASA Programs and include extensive data or theoretical analysis. Includes compilations of significant scientific and technical data and information deemed to be of continuing reference value. NASA counter-part of peer-reviewed formal professional papers but has less stringent limitations on manuscript length and extent of graphic presentations.

- TECHNICAL MEMORANDUM. Scientific and technical findings that are preliminary or of specialized interest, e.g., quick release reports, working papers, and bibliographies that contain minimal annotation. Does not contain extensive analysis.

- CONTRACTOR REPORT. Scientific and technical findings by NASA-sponsored contractors and grantees.

- CONFERENCE PUBLICATION. Collected papers from scientific and technical conferences, symposia, seminars, or other meetings sponsored or co-sponsored by NASA.

- SPECIAL PUBLICATION. Scientific, technical, or historical information from NASA programs, projects, and missions, often concerned with subjects having substantial public interest.

- TECHNICAL TRANSLATION. English-language translations of foreign scientific and technical material pertinent to NASA's mission.

Specialized services also include organizing and publishing research results, distributing specialized research announcements and feeds, providing information desk and personal search support, and enabling data exchange services.

For more information about the NASA STI program, see the following:

- Access the NASA STI program home page at http://www.sti.nasa.gov

- E-mail your question to help@sti.nasa.gov

- Phone the NASA STI Information Desk at 757-864-9658

- Write to:
  NASA STI Information Desk
  Mail Stop 148
  NASA Langley Research Center
  Hampton, VA 23681-2199

NASA/TP–2020-220562

Re-Computation of Numerical Results Contained in NACA Report No. 685

Boyd Perry, III
Langley Research Center, Hampton, Virginia

National Aeronautics and
Space Administration

Langley Research Center
Hampton, Virginia 23681-2199

February 2020

Acknowledgment

The author wishes to acknowledge the valuable contributions to this paper made by Mr. G. Lee Pollard of NCI Information Systems, Inc. Mr. Pollard is a very talented graphic designer. He assembled the recomputed results generated by the present author, electronically scanned the original figures and graphs from *NACA 685*, and merged the former with the latter to produce the final figures and graphs in this paper. Mr. Pollard's skill and enthusiasm made my interactions with him not only very productive, but also very enjoyable. Many thanks!

Available from:

NASA STI Program / Mail Stop 148
NASA Langley Research Center
Hampton, VA 23681-2199
Fax: 757-864-6500

ABSTRACT

In an engineering note published in the Journal of Aircraft in the year 2000, Thomas A. Zeiler made generally known that some of the early works on aeroelastic flutter by Theodore Theodorsen and I.E. Garrick (NACA Report Nos. 496, 685, and 741) contained numerical errors in some of their numerical examples. Some of the plots containing numerical errors were later reproduced in two classic aeroelasticity texts (BAH and BA). Because these foundational papers and texts are often used in graduate courses on aeroelasticity, Zeiler recommended that an effort be undertaken to employ the computational resources available today (digital computers) to recompute the example problems in these early works and to publish the results to provide a complete and error-free set of numerical examples. This paper presents recomputed theoretical results contained in NACA Report No. 685 (*NACA 685*), "Mechanism of Flutter, A Theoretical and Experimental Investigation of the Flutter Problem," by Theodore Theodorsen and I.E. Garrick. The recomputations were performed employing the solution method described in *NACA 685*, but using modern computational tools. With some exceptions, the magnitudes and trends of the original results were in good-to-excellent agreement with the recomputed results, a surprising but gratifying result considering that the *NACA 685* results were computed "by hand" using pencil, paper, slide rules, and mechanical calculators called comptometers. Checks on the recomputations (about 25% were checked) were performed using the so-called p-method of flutter solution. In all cases, including those where the original and recomputed results differed significantly, the checks were in excellent agreement with the recomputed results.

THIS PAGE INTENTIONALLY LEFT BLANK.

I. INTRODUCTION

In a year 2000 engineering note, Zeiler (ref. 1) pointed out that several of the foundational papers and texts in aeroelastic flutter (refs. 2-6) contain numerical errors in some of their example problems. It is not surprising that such errors exist because – especially in the cases of references 2, 3, and 4, written in the 1930s and 40s – all calculations were performed "by hand" using pencil, paper, slide rules, and mechanical calculators called comptometers. References 2, 3, and 4 are Theodore Theodorsen's and I.E. Garrick's groundbreaking "trilogy" of NACA technical reports on aeroelastic flutter. Years after the publication of this trilogy, two classic aeroelasticity texts (refs. 5 and 6) reproduced some of the erroneous figures from reference 3. Because these foundational papers and texts are often used in graduate courses on aeroelasticity, Zeiler recommended that an effort be undertaken to employ the computing resources available today to recompute the numerical examples and to publish the results so as to provide a complete and error-free set of results.

The present paper is the second of three planned papers by the present author that follows Zeiler's recommendation. It contains recomputations of all the numerical examples predicting flutter in reference 3 – NACA Report No. 685, "Mechanism of Flutter, A Theoretical and Experimental Investigation of the Flutter Problem," by Theodorsen and Garrick (referred to hereinafter simply as "*NACA 685*"). The first paper (ref. 7) performed recomputations of all the numerical examples in reference 2; the third paper will do the same for reference 4.

Zeiler stated in his engineering note: "One does not set about lightly to correct the masters …" Embracing this notion, the recomputations contained herein have been carefully checked and rechecked and then checked again using an independent flutter solution method (the p-method, ref. 8). In all cases, including those where the original and present recomputed results differed significantly, the independent results were in excellent agreement with the recomputed results, giving confidence in the recomputed results.

The remainder of this paper is arranged in major sections (many of which contain subsections and sub-subsections) as follows:

Section II presents nomenclature;
Section III presents an overview of *NACA 685*;
Section IV describes the implementation of the *NACA 685* solution method;
Section V describes the numerical checks of the recomputed results;
Section VI describes the manner of comparing the original and recomputed results;
Section VII contains the recomputations and comparisons of results for the figures in *NACA 685*;
Section VIII contains the recomputations and comparisons of results for the graphs in *NACA 685*;
Section IX describes a recurring difference between the original and recomputed results;
Section X contains concluding remarks;
Appendix A presents brief descriptions of Theodorsen's and Garrick's trilogy of papers on flutter;
Appendix B presents comparisons of Zeiler's recomputations with present recomputations.

II. NOMENCLATURE

The symbols in this list are either identical to or consistent with the symbols used in *NACA 685*.

A_{ij}	*ij*-th coefficient in the equations of motion, complex
a	nondimensional distance from midchord to e.a., positive aft
b	semichord, ft
C_h	stiffness in wing deflection, per unit length
C_α	torsional stiffness of wing about e.a., per unit length
C_β	torsional stiffness of aileron about hinge, per unit length
c	nondimensional distance from midchord to aileron hinge, positive aft
e	base of natural logarithms
g_h	structural damping coefficient for deflection mode
g_α	structural damping coefficient for torsion mode
g_β	structural damping coefficient for aileron deflection mode
h	vertical deflection degree of freedom, positive down
h_0	infinitesimal amplitude of h, positive down
i	square root of -1
I_{ij}	imaginary part of A_{ij}
k	reduced frequency, $\omega b/v$
k_f	flutter reduced frequency, $\omega_f b/v_f$
M	mass of wing per unit length, slugs per foot
R_{ij}	real part of A_{ij}
r_r	nondimensional reference length
r_α	nondimensional radius of gyration of wing-aileron about e.a.
r_β	nondimensional radius of gyration of aileron about aileron hinge
T_i	constants from integration of velocity potentials
v	velocity, fps
v_f	flutter velocity, fps
X	nondimensional quantity resulting from normalizing equations of motion, $\frac{1}{\kappa}\left(\frac{br_r\omega_r}{vk}\right)^2$
x_α	nondimensional distance from e.a. to c.g. of wing-aileron, positive aft
x_β	nondimensional distance from aileron hinge to c.g. of aileron, positive aft
α	torsion degree of freedom, positive leading edge up
α_0	infinitesimal amplitude of α, positive leading edge up
β	aileron deflection degree of freedom, positive trailing edge down with respect to wing
β_0	infinitesimal amplitude of β, positive trailing edge down with respect to wing
κ	mass ratio, $\frac{\pi\rho b^2}{M}$
ρ	mass of air per unit volume, slugs per cubic foot
ξ	modal-coupling factor
φ_0	phase angle of α with respect to an unspecified reference, radians

φ_1 phase angle of β with respect to an unspecified reference, radians

φ_2 phase angle of h with respect to an unspecified reference, radians

ω circular frequency, rps

ω_f flutter frequency, rps

ω_h natural frequency of wing-deflection mode, rps

ω_r reference frequency, rps

ω_α natural frequency of wing-torsion mode, rps

ω_β natural frequency of aileron-deflection mode, rps

Ω_h square of nondimensional frequency ratio, $\left(\frac{\omega_h}{\omega_r r_r}\right)^2$

Ω_α square of nondimensional frequency ratio, $\left(\frac{\omega_\alpha r_\alpha}{\omega_r r_r}\right)^2$

Ω_β square of nondimensional frequency ratio, $\left(\frac{\omega_\beta r_\beta}{\omega_r r_r}\right)^2$

Abbreviations:

c.g. center of gravity

e.a. elastic axis

fps feet per second

NACA National Advisory Committee for Aeronautics

rps radians per second

2DOF two degrees of freedom

3DOF three degrees of freedom

Dots over symbols denote derivatives with respect to time.

Some of the quantities in the nomenclature list and their positive senses are illustrated in the following sketch, taken from *NACA 685*:

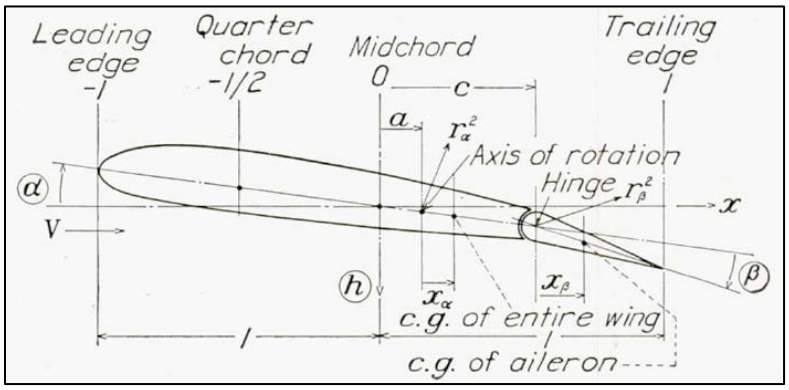

III. OVERVIEW OF NACA REPORT NO. 685

The first sentence of the Summary in *NACA 685* states "The results of the basic flutter theory originally devised in 1934 and published as NACA Technical Report No. 496 are presented in a simpler and more complete form for further studies." "Simpler" is addressed in the Solution Method subsection of this section of the paper. "More complete" includes: (1) the addition of structural damping and a modal coupling factor to the equations of motion, thereby incorporating additional physics into the equations that more realistically represents a three dimensional wing; (2) an extensive set of parameter variations in its example problems for flutter involving two degrees of freedom; (3) example problems for flutter involving three degrees of freedom; (4) the inclusion of many more experimental results, including flutter and ground tests; and (5) discussions on airplane flutter and air damping of forced vibrations.

The five subsections that follow address the theoretical development, the solution method, comments by the present author on the solution method, the tables contained in *NACA 685*, and the figures and graphs contained in *NACA 685*. Because the theoretical development in *NACA 685* is so similar to that in reference 2, portions of the subsection immediately below are very similar to a comparable section in reference 7.

NACA 685 Theoretical Development

The equations of motion used in *NACA 685* are those from reference 2 for a typical section with degrees of freedom in torsion (α), aileron deflection (β), and vertical deflection (sometimes referred to as flexure) (h). These equations are three second-order differential equations in the three unknowns α, β, and h, and their first and second time derivatives. They are comprised of aerodynamic, inertia, and restraining terms.

$$\text{(A)}\quad \ddot{\alpha}\left[r_\alpha^2+\kappa\left(\frac{1}{8}+a^2\right)\right]+\dot{\alpha}\frac{v}{b}\kappa\left(\frac{1}{2}-a\right)+\alpha\frac{C_\alpha}{Mb^2}+\ddot{\beta}\left[r_\beta^2+(c-a)x_\beta-\frac{T_7}{\pi}\kappa-(c-a)\frac{T_1}{\pi}\kappa\right]+\frac{1}{\pi}\dot{\beta}\kappa\frac{v}{b}\left[-2p-\left(\frac{1}{2}-a\right)T_4\right]$$
$$+\beta\kappa\frac{v^2}{b^2}\frac{1}{\pi}(T_4+T_{10})+\ddot{h}\left(x_\alpha-a\kappa\right)\frac{1}{b}-2\kappa\left(a+\frac{1}{2}\right)\frac{vC(k)}{b}\left[\frac{v\alpha}{b}+\frac{\dot{h}}{b}+\left(\frac{1}{2}-a\right)\dot{\alpha}+\frac{T_{10}}{\pi}\frac{v}{b}\beta+\frac{T_{11}}{2\pi}\dot{\beta}\right]=0$$

$$\text{(B)}\quad \ddot{\alpha}\left[r_\beta^2+(c-a)x_\beta-\kappa\frac{T_7}{\pi}-(c-a)\frac{T_1}{\pi}\kappa\right]+\dot{\alpha}\left(p-T_1-\frac{1}{2}T_4\right)\frac{v}{b}\frac{\kappa}{\pi}+\ddot{\beta}\left(r_\beta^2-\frac{1}{\pi^2}\kappa T_3\right)-\frac{1}{2\pi^2}\dot{\beta}T_4T_{11}\frac{v}{b}\kappa$$
$$+\beta\left[\frac{C_\beta}{Mb^2}+\frac{1}{\pi^2}\frac{v^2}{b^2}\kappa(T_5-T_4T_{10})\right]+\ddot{h}\left(x_\beta-\frac{1}{\pi}\kappa T_1\right)\frac{1}{b}+\frac{T_{12}}{\pi}\kappa\frac{vC(k)}{b}\left[\frac{v\alpha}{b}+\frac{\dot{h}}{b}+\left(\frac{1}{2}-a\right)\dot{\alpha}+\frac{T_{10}}{\pi}\frac{v}{b}\beta+\frac{T_{11}}{2\pi}\dot{\beta}\right]=0$$

$$\text{(C)}\quad \ddot{\alpha}\left(x_\alpha-\kappa a\right)+\dot{\alpha}\frac{v}{b}\kappa+\ddot{\beta}\left(x_\beta-\frac{1}{\pi}T_1\kappa\right)-\dot{\beta}\frac{v}{b}T_4\kappa\frac{1}{\pi}+\ddot{h}\,(1+\kappa)\frac{1}{b}+h\frac{C_h}{M}\frac{1}{b}$$
$$+2\kappa\frac{vC(k)}{b}\left[\frac{v\alpha}{b}+\frac{\dot{h}}{b}+\left(\frac{1}{2}-a\right)\dot{\alpha}+\frac{T_{10}}{\pi}\frac{v}{b}\beta+\frac{T_{11}}{2\pi}\dot{\beta}\right]=0$$

Equations (A), (B), and (C) are reproduced from reference 2. Equation (A) defines the sum of the moments about the elastic axis; equation (B), the sum of the moments about the aileron hinge; and equation (C), the sum of the forces on the entire "wing" in the vertical direction. Unsteady circulatory

aerodynamics are present in the equations in the form of Theodorsen's circulation function, $C(k)$, a complex function of reduced frequency, k, comprised of Bessel functions of the first and second kind.

NACA 685 takes these equations and then adds to each structural damping, g, and, for the two-degrees-of-freedom subsets of these equations, adds a modal coupling factor, ξ. These additions will be addressed below.

Assumed forms of the unknowns α, β, and h. – The assumed form of the unknowns in equations (A), (B), and (C) is sinusoidal:

$$\alpha = \alpha_0 e^{i(k\frac{v}{b}t+\varphi_0)} \tag{1a}$$

$$\beta = \beta_0 e^{i(k\frac{v}{b}t+\varphi_1)} \tag{1b}$$

$$h = h_0 e^{i(k\frac{v}{b}t+\varphi_2)} \tag{1c}$$

where α_0, β_0, and h_0 are the (infinitesimal) amplitudes of α, β, and h, and φ_0, φ_1 and φ_2 are phase angles with respect to an unspecified reference. The first and second time derivatives of α, β, and h are:

$$\dot{\alpha} = ik\frac{v}{b}\alpha \text{ and } \ddot{\alpha} = -\left(k\frac{v}{b}\right)^2\alpha$$

$$\dot{\beta} = ik\frac{v}{b}\beta \text{ and } \ddot{\beta} = -\left(k\frac{v}{b}\right)^2\beta$$

$$\dot{h} = ik\frac{v}{b}h \text{ and } \ddot{h} = -\left(k\frac{v}{b}\right)^2 h.$$

Substitution of assumed forms into, and normalization of, equations. – Making the substitutions of equations (1a) through (1c) and their time derivatives into equations (A) through (C) transforms the latter equations from three simultaneous differential equations into three simultaneous algebraic equations with complex coefficients. The algebraic equations are then normalized by the quantity $\kappa\left(\frac{v}{b}k\right)^2$, resulting in the equations taking the form

$$(A_{a\alpha} + \Omega_\alpha X)\alpha + A_{a\beta}\beta + A_{ah}h = 0 \tag{2a}$$

$$A_{b\alpha}\alpha + (A_{b\beta} + \Omega_\beta X)\beta + A_{bh}h = 0 \tag{2b}$$

$$A_{c\alpha}\alpha + A_{c\beta}\beta + (A_{ch} + \Omega_h X)h = 0. \tag{2c}$$

The quantity $A_{a\alpha}$ and all other similar quantities contain both aerodynamic and structural contributions. They are complex functions of reduced frequency, with real parts $R_{a\alpha}$ (and all similar real parts) and imaginary parts $I_{a\alpha}$ (and all similar imaginary parts).

The physical parameters of the problem (a, b, c, $\kappa, x_\alpha, r_\alpha, x_\beta, r_\beta, \omega_\alpha, \omega_\beta$, and ω_h) reside in the A_{ij} and $\Omega_j X$ terms.

Products $\Omega_\alpha X$, $\Omega_\beta X$, and $\Omega_h X$. – In equations (2a), (2b), and (2c) the products $\Omega_\alpha X$, $\Omega_\beta X$, and $\Omega_h X$ are real. They are derived from quantities $\frac{C_\alpha}{Mb^2}$ (from eqn. (A)), $\frac{C_\beta}{Mb^2}$ (from eqn. (B)), and $\frac{C_h}{Mb}$ (from eqn. (C)), respectively. Via the substitution and rearrangement of terms and the use of cancelling expressions in the numerator and denominator, from reference 2, these products are

$$\Omega_\alpha X = \frac{C_\alpha}{k^2 M v^2 \kappa} = \left(\frac{\omega_\alpha r_\alpha}{\omega_r r_r}\right)^2 \frac{1}{\kappa}\left(\frac{b r_r \omega_r}{vk}\right)^2 \tag{3a}$$

$$\Omega_\beta X = \frac{C_\beta}{k^2 M v^2 \kappa} = \left(\frac{\omega_\beta r_\beta}{\omega_r r_r}\right)^2 \frac{1}{\kappa}\left(\frac{b r_r \omega_r}{vk}\right)^2 \tag{3b}$$

$$\Omega_h X = \frac{C_h b^2}{k^2 M v^2 \kappa} = \left(\frac{\omega_h}{\omega_r r_r}\right)^2 \frac{1}{\kappa}\left(\frac{b r_r \omega_r}{vk}\right)^2 \tag{3c}$$

where, to the right of the second equal sign in each equation, X comprises the two right-most terms

$$X = \frac{1}{\kappa}\left(\frac{b r_r \omega_r}{vk}\right)^2. \tag{4}$$

The respective Ω_j, the remaining terms, are

$$\Omega_\alpha = \left(\frac{\omega_\alpha r_\alpha}{\omega_r r_r}\right)^2 \tag{5a}$$

$$\Omega_\beta = \left(\frac{\omega_\beta r_\beta}{\omega_r r_r}\right)^2 \tag{5b}$$

$$\Omega_h = \left(\frac{\omega_h}{\omega_r r_r}\right)^2. \tag{5c}$$

The quantities ω_r and r_r are a reference frequency and a reference length, which may be conveniently chosen.

Referring back to the normalization that produced equations (2a) through (2c), a critically important result is that the quantity X has been conveniently isolated from the other terms in these equations and it is the only quantity in these equations that contains the velocity. Therefore, solving these equations for X determines the flutter velocity, v_f. As will be seen later, X is a clever artifice created by Theodorsen. At times, X is treated not as the known quantity defined in equation (4), but rather as a parameter; at other times, X is treated as a known quantity.

Addition of structural damping, g, to the equations of motion. – *NACA 685* employs structural damping as "… a force in phase with the velocity but of a magnitude proportional to the restoring force." It identifies the restoring forces as the stiffness terms multiplied by their respective displacements ($C_\alpha \alpha$, $C_\beta \beta$, and $C_h h$) in equations (A), (B), and (C).

The stiffness terms C_α, C_β, and C_h are also seen to reside in equations 3(a), 3(b), and 3(c). Thus, to incorporate the structural damping forces into the equations of motion merely requires that factors $(1 + ig_\alpha)$, $(1 + ig_\beta)$, and $(1 + ig_h)$ multiply terms C_α, C_β, and C_h, respectively. Within the parentheses, the "1" denotes the stiffness terms already present in the equations and the "$+ig$" denotes the added structural damping terms. When these factors are included, the following modified form of the equations of motion results

$$(A_{a\alpha} + \Omega_\alpha(1 + ig_\alpha)X)\alpha + A_{a\beta}\beta + A_{ah}h = 0 \tag{6a}$$

$$A_{b\alpha}\alpha + (A_{b\beta} + \Omega_\beta(1 + ig_\beta)X)\beta + A_{bh}h = 0 \tag{6b}$$

$$A_{c\alpha}\alpha + A_{c\beta}\beta + (A_{ch} + \Omega_h(1 + ig_h)X)h = 0. \tag{6c}$$

Modal coupling factor, ξ, added to the two-degrees-of-freedom form of the equations of motion. – *NACA 685* devotes much of its content to examining flutter solutions for the three two-degrees-of-freedom (2DOF) subsets available from the three-degrees-of-freedom (3DOF) equations of motion: flexure-torsion, involving h and α (referred to in *NACA 685* as Case 1); aileron-flexure, involving β and h (Case 2); and torsion-aileron, involving α and β (Case 3).

To the 2DOF subsets, *NACA 685* introduces what it calls a "coupling factor," ξ. (To more accurately describe its function the present author prefers the term "modal coupling factor.") The modal coupling factor is intended to approximate, for a typical section (a two-dimensional entity), the effects of three-dimensional geometries present on real wings. The modal coupling factor represents the condition "… in which only a part of the total length of the (infinitely long) wing is given the second degree of freedom." An obvious application of the modal coupling factor is an aileron that is not full span. (In fact, in ref. 4, the third paper of the trilogy, Theodorsen and Garrick change terminology and refer to ξ as the "aileron coefficient.")

In *NACA 685*, the modal coupling factor appears as a multiplier on the upper-right off-diagonal term of the 2DOF equations of motion, as shown in the following example using the torsion-aileron equations

$$(A_{a\alpha} + \Omega_\alpha(1 + ig_\alpha)X)\alpha + \xi A_{a\beta}\beta = 0 \tag{7a}$$

$$A_{b\alpha}\alpha + (A_{b\beta} + \Omega_\beta(1 + ig_\beta)X)\beta = 0 \tag{7b}$$

where equations (7a) and (7b) correspond to equations (6a) and (6c), respectively, but without degree of freedom h and its associated coefficients. Equivalently, the modal coupling factor could have appeared instead as a multiplier on the lower-left off-diagonal term. The modal coupling factor takes on values from zero (no coupling) to one (full coupling).

It should be emphasized that, through their respective off-diagonal terms, modal coupling is naturally present in equations (2a), (2b), and (2c), equations (6a), (6b), and (6c), and equations (7a) and (7b). The modal coupling factor is a "manufactured" empirical quantity whose function is to attenuate the modal

coupling naturally present. In *NACA 685*, the authors employ the modal coupling factor in the 2DOF equations only, but there is nothing to preclude its use in the 3DOF equations.

NACA 685 Solution Method

In reference 2, two solution methods are presented: one for solving the three-degrees-of-freedom (3DOF) flutter equations (never actually implemented in ref. 2); and another for solving the two-degrees-of-freedom (2DOF) flutter equations. The former is more straightforward, but requires the solution of a cubic equation; the latter is more clever and ingenious, but is complicated and cumbersome to implement.

NACA 685 employs the 3DOF solution method of reference 2 for solving both the 3DOF and 2DOF flutter equations. It is this solution method that the authors of *NACA 685* refer to in the Summary of *NACA 685* when they say "… the basic flutter theory [is] … simpler …" than the one implemented in reference 2. Indeed it is.

For the 3DOF flutter equations, the solution of equations (6a), (6b), and (6c) is obtained when their determinant is zero

$$\begin{vmatrix} A_{a\alpha} + \Omega_\alpha(1+ig_\alpha)\,X & A_{a\beta} & A_{ah} \\ A_{b\alpha} & A_{b\beta} + \Omega_\beta(1+ig_\beta)\,X & A_{bh} \\ A_{c\alpha} & A_{c\beta} & A_{ch} + \Omega_h\,(1+ig_h)X \end{vmatrix} = 0. \tag{8}$$

Expanding the determinant in equation (8) yields a complex cubic equation in X.

Rather than solving this complex cubic equation directly, *NACA 685* offers the computational shortcut of creating two equations, each equal to zero and each with real coefficients, by separating the real and imaginary parts of the original equation. The "real" equation is comprised of the real parts of the expansion of equation (8); the "imaginary" equation is comprised of the imaginary parts. Because of the presence of structural damping, both the real and imaginary equations are cubic in X. If structural damping is not present, the real equation is still cubic but the imaginary equation becomes quadratic.

For the 2DOF flutter equations, using equations (7a) and (7b) (without ξ) as the example, the solution is obtained when their determinant is zero

$$\begin{vmatrix} A_{a\alpha} + \Omega_\alpha(1+ig_\alpha)\,X & A_{a\beta} \\ A_{b\alpha} & A_{b\beta} + \Omega_\beta\,(1+ig_\beta)X \end{vmatrix} = 0. \tag{9}$$

Expanding the determinant in equation (9) yields a complex quadratic equation in X.

At this point, as with the 3DOF equations, a similar separation of the real and imaginary parts occurs resulting in real and imaginary equations that are quadratic in X. If structural damping is not present, the real equation is still quadratic but the imaginary equation becomes linear.

The *NACA 685* solution method is a straightforward four-step process aimed at finding the flutter velocity, v_f, and the flutter reduced frequency, k_f, that simultaneously solve both the real and imaginary equations, and therefore, also solves the original equation with complex coefficients:

Step 1: Solve real and imaginary equations for X. – The artifice of treating X as a parameter, rather than as a known quantity, is employed. The real and imaginary equations are each solved for X for many values of the inverse of reduced frequency, $1/k$. The roots of each equation are plotted on the same set of axes as functions of $1/k$, with each equation producing the same number of loci as the order of the respective equation. (These loci are not what are commonly referred to as classical root loci.) Each point of each real locus is a solution of the real equation; each point of each imaginary locus is a solution of the imaginary equation. (Later, in the present paper, plots of this form are referred to as "raw form" illustrations of the *NACA 685* solution method.)

Step 2: Identify intersections of real and imaginary loci. – Intersections of any of the real loci with any of the imaginary loci are simultaneous solutions of both equations, and therefore, are also solutions of the original equation with complex coefficients, thus supplying pairs of values, X and $1/k$, that satisfy the original equation. However, these pairs of X and $1/k$ are not necessarily flutter solutions. Because, X is proportional to the inverse square of velocity (eqn. (4)), only those intersections of the loci involving real positive values of X (and therefore real – not complex or imaginary – velocities) are flutter solutions. These intersections will be termed "proper intersections" and the corresponding pairs of X and $1/k$ will be termed "proper pairs." After proper intersections and pairs have been determined, the artifice of treating X as a parameter is abandoned. (The term "proper" in this context is an invention of the present author and is not found in *NACA 685*.)

Step 3: Identify flutter reduced frequency. – From each proper pair, its flutter reduced frequency, k_f, is determined from the inverse of $1/k$.

Step 4: Identify flutter velocity. – From each proper pair, its flutter velocity is determined by rearranging equation (4) and solving for velocity

$$v_f = \frac{1}{\sqrt{\kappa}} \frac{b\omega_r r_r}{k_f} \frac{1}{\sqrt{X}} . \tag{10}$$

The value of k_f from Step 3, its corresponding value of X, and the problem-specific quantities κ, b, r_r, and ω_r are substituted into equation (10), yielding the flutter velocity. Multiple proper intersections and pairs produce multiple flutter solutions.

Comments on *NACA 685* Solution Method

This subsection of the paper offers some comments by the present author on the solution method of *NACA 685*.

Use of the inverse of the reduced frequency. – As stated in Step 1, above, the solution method sweeps on the inverse of the reduced frequency, $1/k$, rather than on the reduced frequency itself. One can imagine a modification of this solution method that would sweep not on the inverse of the reduced frequency, but on the reduced frequency. This modified solution method would produce the same results. But, at proper intersections, it would have the benefit of indicating directly the flutter reduced frequency by avoiding the necessity of inverting the inverse of the reduced frequency, as is currently done in Step 3. Theodorsen and Garrick offered no explanation in reference 3 regarding why they chose the inverse of the reduced frequency as their independent variable. In addition, their solution methods in references 2 and 4 also sweep on $1/k$, also without explanation; and in figure 4 of reference 2, F and G, the real and imaginary parts of the Theodorsen circulation function, are plotted as functions of $1/k$. So, clearly, they preferred the inverse of the reduced frequency over the reduced frequency.

No knowledge of subcritical damping. – Modern flutter solution methods predict the subcritical damping of the flutter mode (and all other modes) as the flutter velocity is approached. The p-method produces a velocity root locus plot from which damping ratios at subcritical velocities are easily found. The k and p-k methods produce directly plots of structural damping as functions of velocity. However, the *NACA 685* solution method predicts only the flutter condition with no knowledge of subcritical damping as the flutter velocity is approached.

Repeated roots in the solution of real and imaginary equations. – Recall that, depending on the number of degrees of freedom and the presence or absence of structural damping, the real equation may be either cubic or quadratic in X and the imaginary equation may be cubic, quadratic, or linear in X. For cubic or quadratic equations (either real or imaginary), repeated roots are possible, which means that in the plotting of the loci (either real or imaginary) as a function of $1/k$, two of the real loci or two of the imaginary loci may approach each other and meet at a point representing the repeated root. This condition will be seen to occur in some of the original and recomputed results.

In a particular numerical example, if a repeated root does exist, to numerically "capture" it requires that the equations be solved at the exact value of $1/k$ that produces the repeated root. In the present implementation of the *NACA 685* solution method (discussed below), values of $1/k$ are chosen in an automated manner, making it extremely unlikely that such an exact value of $1/k$ would be found. In sweeping through $1/k$, it would therefore be extremely likely that that exact value of $1/k$ would be skipped over, meaning that, when plotted, the two loci that would approach each other and otherwise meet at the repeated root, would instead approach each other but then stop short of actually meeting. This will be seen to be the case for some of the recomputed results.

Tables in *NACA 685*

NACA 685 contains several tables at the back of the report, some identified with Arabic numerals, others with Roman numerals.

***NACA 685* Tables identified with Arabic numerals**. – *NACA 685* Tables 1, 2, 3, and 4 contain a variety of precomputed quantities intended to aid the reader of *NACA 685* in solving numerical examples.

NACA 685 Table 1 lists the real and the negative of the imaginary parts of the Theodorsen circulation function, F and $-G$, and quantities $-2G/k$ and $2F/k^2$ for 30 values of $1/k$ between zero and infinity.

NACA 685 Table 2 contains values of the various T_i, the constants obtained from the integration of velocity potentials, for 13 values of c, the nondimensional distance from midchord to aileron hinge.

NACA 685 Table 3 contains values of the real and imaginary parts of $A_{a\alpha}$ for seven values of a, the nondimensional distance from midchord to the elastic axis, and for 26 values of $1/k$ between zero and 20.

NACA 685 Table 4 contains values of the real and imaginary parts of $A_{b\beta}$ for 11 of the 13 values of c contained in Table 2 and for 23 values of $1/k$ between zero and 10.

The following table shows the values of $1/k$ contained in Tables 1, 3, and 4 of *NACA 685*:

Table 1	Table 3	Table 4
0	0	0
0.1	0.1	0.1
0.16667	0.16667	0.16667
0.25	0.25	0.25
0.33333	0.33333	0.33333
0.5	0.5	0.5
0.66667	0.66667	0.66667
0.83333	0.83333	0.83333
1	1	1
1.25	1.25	1.25
1.51516	1.51516	1.51516
1.66667	1.66667	1.66667
1.78572	1.78572	1.78572
2	2	2
2.27273	2.27273	2.27273
2.5	2.5	2.5
2.94118	2.94118	2.94118
3.33333	3.33333	3.33333
4.16667	4.16667	4.16667
5	5	5
6.25	6.25	6.25
8.33333	8.33333	8.33333
10	10	10
12.5	12.5	
16.66667	16.66667	
20	20	
25		
40		
100		
∞		

These values of $1/k$ will be referred to as Theodorsen's and Garrick's tabular values of $1/k$. No explanation is given in *NACA 685* regarding why its Tables 1, 3, and 4 contain different numbers of reduced frequencies.

***NACA 685* Tables identified with Roman numerals**. – *NACA 685* Tables I and IA contain information pertinent to the experimental flutter investigations reported in *NACA 685*. Each table contains wind-tunnel model physical dimensions, including structural frequencies, wind-tunnel test conditions, flutter velocities and frequencies, and remarks.

Figures and Graphs in *NACA 685*

NACA 685 contains "figures" and "graphs." Eleven of the 39 figures in *NACA 685* illustrate flutter solutions and are of interest herein; the remainder of the figures address other things. These eleven figures may contain either 2DOF or 3DOF examples. There are three graphs in *NACA 685*, all of which illustrate 2DOF flutter solutions. All graphs contain multiple parts, with each part containing at least one parametric variation.

As stated elsewhere in the present paper, the calculations required to produce the original figures and graphs were performed "by hand" with pencil, paper, slide rules, and comptometers. By their nature, these calculations were intricate, multistepped, and very time consuming. To produce a single flutter prediction would have taken hours of careful calculating and precise hand plotting. The figures and graphs in *NACA 685* contain hundreds of flutter predictions produced in this way.

With one exception (part (a) of Graph I-B), the original results in *NACA 685* are presented as continuous curves, not discrete points. To produce these continuous curves, first, discrete points were obtained and plotted, and second, the curves were constructed by fairing through the points. The authors of *NACA 685* never say how many discrete points they employed in their curves, and, after almost eight decades since the publication of *NACA 685*, it is unlikely that that particular detail will ever be known.

IV. IMPLEMENTATION OF *NACA 685* SOLUTION METHOD

The implementation of the four-step *NACA 685* solution method was accomplished by the present author via the writing and execution of m-files in Matlab®. Recomputations were performed using these m-files. The real and imaginary equations were solved for X using the Matlab® "roots" function over a range of the inverse of reduced frequency. Proper intersections were identified using a linear interpolation scheme. Typically, the lower value of $1/k$ was 0.01, the upper value was 100, and the distribution was logarithmic. The total number of values varied depending on the nature of the real and imaginary loci, but, for the case of 1000 values of $1/k$ over a range of four orders of magnitude, successive values of $1/k$ were 1.0093 times larger than the previous value and each decade within the distribution contained 250 values of $1/k$.

Advantage of the Present Implementation over the Original Implementation

The original implementation of the *NACA 685* solution method was performed "by hand," while the present implementation was performed on a desktop computer. At the "cost" of a few seconds of

computation time, the present implementation can produce hundreds of solutions at very fine increments in the inverse of reduced frequency, assuring accurate identifications of $1/k$ and $\sqrt{X}$ at proper intersections. Because it was performed by hand, the original implementation was restricted to as few reduced frequencies as the authors of *NACA 68*5 determined to be practical to identify $1/k$ and $\sqrt{X}$. As will be seen in Section VII of the present paper, below, this restriction, dictated by practicality, sometimes resulted in small absolute differences between the original and recomputed values of $1/k$ at proper intersections, which could produce large percentage differences in values of v_f and k_f.

Complication in the Present Implementation

All original figures and graphs in *NACA 685* contain at least one result for which either all structural damping coefficients (g_α, g_β, and g_h) are zero and/or a natural frequency ratio (meaning, necessarily, that one of Ω_α, Ω_β, or Ω_h) is zero. In the present implementation of the *NACA 685* solution method, either of these conditions caused the "roots" function to crash and, as a consequence, the solution method failed to produce a solution. This difficulty was easily circumvented by employing an approximation: substituting small non-zero values in place of the offending quantities (zeros).

The difficulty and circumvention are best understood by taking as an example the 3DOF flutter problem, where the real and imaginary equations are cubic. In these equations, the coefficients of X^3 are –

– for the real equation: $\Omega_\alpha\Omega_\beta\Omega_h\left(1 - g_\alpha g_\beta - g_\beta g_h - g_h g_\alpha\right)$

– for the imaginary equation: $\Omega_\alpha\Omega_\beta\Omega_h\left(g_\alpha + g_\beta + g_h - g_\alpha g_\beta g_h\right)$.

For the condition of zero structural damping coefficients, the X^3 coefficient in the imaginary equation is zero; for the condition of a zero frequency ratio, the X^3 coefficient in both equations is zero. If the coefficient of the highest-order term is zero, the "roots" function crashes.

So that the solution method would yield a solution, structural damping coefficients of zero were approximated by the value $1\text{x}10^{-8}$; and a natural frequency ratio of zero was approximated by the value 0.001. Both of these approximations produced nonzero values of the coefficients of X^3 in the real and imaginary equations and prevented the "roots" function from crashing.

V. NUMERICAL CHECKS OF RECOMPUTED RESULTS

Recomputed numerical results (flutter velocities and flutter reduced frequencies) were spot-checked using an independent flutter solution method – the p-method of flutter solution (ref. 8). The p-method was written and coded in Matlab® by the present author following the formulation outlined in Appendix B of reference 9.

The present implementation of the p-method employs the following fourth-order-over-fourth-order approximation of Theodorsen's circulation function

$$C(k) \approx \frac{0.5(ik)^4 + 0.703(ik)^3 + 0.2393(ik)^2 + 0.01894(ik) + 0.0002318}{(ik)^4 + 1.158(ik)^3 + 0.3052(ik)^2 + 0.02028(ik) + 0.0002325} \tag{11}$$

identified in reference 10 as the "balanced truncation" approximation. This approximation is excellent. Over the range of reduced frequency $0.001 < k < 10$, it approximates the complex modulus of $C(k)$ to within 0.3 percent and approximates the phase angle of $C(k)$ to within 0.25 degrees.

[A brief aside regarding the approximation expressed in equation (11): One would reasonably expect the ratio of the coefficients of the $(ik)^4$ terms in the numerator and denominator to be one-half so that the value of the approximation as $k \to \infty$ would exactly match the value of Theodorsen's circulation function as $k \to \infty$. This is the case. One would also reasonably expect the ratio of the constant terms in the numerator and denominator to be unity so that the value of the approximation at $k = 0$ would exactly match the value of Theodorsen's circulation function at $k = 0$. This is not the case; the ratio of the coefficients in the approximation is 0.997. There is no reason offered in reference 10 regarding why this ratio is not unity.]

An advantage of the p-method is that it produces a classical root locus in the Laplace domain. In circumstances where the *NACA 685* solution method produced multiple flutter conditions (i.e., multiple proper intersections) the p-method was ideal for determining the nature of those flutter conditions – for example, whether there were two separate flutter modes, each of which went unstable and remained unstable with increasing velocity, or whether the intersections corresponded to a "hump mode" that went unstable at one velocity but then restabilized at a higher velocity. (As will be seen later in this paper, the solution method of *NACA 685* does correctly identify both conditions – destabilizing and restabilizing – that define a hump mode.)

Generally, one out of every three or four recomputed results was checked using the p-method. In almost all instances, the spot-checked answers (flutter velocity and flutter reduced frequency) were within 0.5 percent of the corresponding answers recomputed by the *NACA 685* solution method (no difference exceeded 2 percent), giving confidence that the recomputed results presented herein are correct.

VI. MANNER OF COMPARISON OF ORIGINAL AND RECOMPUTED RESULTS

This section of the paper addresses the manner in which the original and recomputed results are compared with each other.

Presentation of Original and Recomputed Results

The eleven figures and three graphs of interest have been electronically scanned and are included in the present paper, retaining their original figure and graph numbers from *NACA 685*. Recomputed results have been superimposed on these originals. Keys have been added to each figure and graph.

To distinguish between the original and recomputed results –

- for figures 1 through 7, the original results are black curves and the recomputed results are blue and red curves;
- for figures 8, 17, 19, and 26, the original results are black curves and the recomputed results are colored symbols;
- for the graphs, the original results are black curves overlaid with color bands specific to a particular value of a physical constant and the recomputed results are symbols in corresponding colors.

Assessment of Agreement Between Original and Recomputed Results

Although precise numerical values of the recomputed results ($1/k$ and $\sqrt{X}$ at proper intersections and the resulting v_f and k_f) were available, those of the original results generally were not available. The original results were generally available in plot form only. Therefore, a quantitative assessment of the agreement between the original and recomputed results in the form of percentage differences was generally not possible. In the absence of a quantitative assessment of agreement, criteria were devised for a qualitative assessment of agreement. Table 1 contains these criteria.

Table 1 is applied in the following ways –

- for figures 1 through 7, because the recomputed results are presented as curves, the center column in Table 1 is not employed;
- for the remaining figures and the graphs, the entirety of Table 1 is employed.

However, some amount of discretion and awareness is required in using Table 1. The figures and graphs that contain symbols representing the recomputed results have many different scales on their respective axes. Therefore, the diameter of a symbol in one figure or graph generally represents a different fraction of the maximum value on the ordinate of that graph than that of another symbol in another figure or graph. For this reason, the qualifiers (excellent, good, fair, poor) are generally not consistent from one figure or graph to another. However, it is felt that within a given figure or graph the criteria in Table 1 provide a convenient and appropriate means of discussing that particular comparison.

VII. RECOMPUTATION AND COMPARISON OF RESULTS CONTAINED IN FIGURES OF *NACA 685*

NACA 685 states that the physical constants pertaining to the examples presented in the figures correspond to "a large modern airplane." With a few exceptions, the figures share the following set of physical constants:

$$a = -0.4;\ b = 6;\ c = 0.6;\ \kappa = 0.25;\ x_\alpha = 0.2;\ r_\alpha^2 = 0.25;\ x_\beta = 0;\ r_\beta^2 = 0.0012;$$

$$\omega_\alpha = 90;\ \left(\frac{\omega_h}{\omega_\alpha}\right)^2 = \frac{1}{16}\ \text{(from which } \omega_h = 22.5);\ \left(\frac{\omega_\beta}{\omega_h}\right)^2 = \frac{3}{2}\ \text{(from which } \omega_\beta = 27.557);$$

$$g_\alpha = 0;\ g_\beta = 0;\ g_h = 0;\ \xi = 1.$$

Table 2 contains a complete listing of all physical constants for all figures. Blank entrees in a row correspond to a particular physical constant not being required for that particular Case.

Raw Form Illustrations of the *NACA 685* Solution Method

Figures 1 through 7 illustrate the *NACA 685* solution method in its raw form, that is, with the loci of the solutions of the real and imaginary equations. In these figures, the ordinate is the square root of X and the abscissa is the inverse of reduced frequency, $1/k$. Only positive values of $\sqrt{X}$ are shown, meaning that all intersections in these figures are proper intersections, and therefore, represent flutter solutions. Figures 1, 4, 5, 6, and 7 contain proper intersections.

For the *NACA 685* original results, the real loci are identified with the letter R and the imaginary loci are identified with the letter I. For recomputed results, these loci are presented as blue and red curves, respectively.

Because there is no structural damping present for any of the examples in these figures, for the 2DOF flutter problems (that is, for Cases 1, 2, and 3), the real and imaginary equations are quadratic and linear, respectively, resulting in two loci and one locus, respectively. For the 3DOF flutter problems, the equations are cubic and quadratic, respectively, resulting in three and two loci, respectively.

Original figures 1 through 7 contain small open circles on some of the loci. In figures 1 through 4, these circles have two meanings: (1) indicating the (positive) values of $\sqrt{X}$ for the real and imaginary loci at the value of $1/k$ of unity; and (2) indicating the proper intersection of a real locus with an imaginary locus. In figures 5, 6, and 7, they indicate proper intersections only.

In the following discussions of figures 1 through 7, it is important and revealing to compare the overall shapes of the original and recomputed real and imaginary loci. However, because they determine the flutter velocity, v_f, and flutter reduced frequency, k_f, it is even more important to compare the original and recomputed proper intersections.

For those figures that contain proper intersections (figs. 1, 4, 5, 6, and 7), Table 3 contains comparisons of the original and recomputed quantities $1/k$, $\sqrt{X}$, v_f, and k_f, as well as calculations of percentage differences for each quantity.

For the original results in figures 1 and 4, values of $1/k$ and $\sqrt{X}$ at proper intersections and the corresponding value of v_f are given in the *NACA 685* text; the corresponding value of k_f is available from the inverse of $1/k$ at the proper intersection. For the original results in figures 5, 6, and 7, values of v_f and k_f were obtained by the present author by reading the values of $1/k$ and $\sqrt{X}$ at proper intersections in the original figures and then employing equation (10). For all recomputed results, values of $1/k$, $\sqrt{X}$, v_f, and k_f are directly available as outputs of the solution method.

Figure 1. – Figure 1 contains raw form results for Case 1, and thus, has two real loci and one imaginary locus. Figure 1 has a single proper intersection, producing a single flutter mode. The two original real loci approach each other and meet at a point, indicating a repeated root. The recomputed real loci

approach each other but do not actually meet at a point for the reason stated in the "Comments on Solution Method" subsection of Section III. Except for the real loci at values of $1/k$ higher than about 3.3, the agreement between all original and recomputed loci is excellent, including the agreement of the respective proper intersections.

The proper intersection from the recomputed results corresponds to a flutter velocity $v_f = 834.2$ feet per second and a flutter reduced frequency $k_f = 0.407$. The original flutter velocity and flutter reduced frequency, obtained by employing equation (10) with the values of $\sqrt{X}$ and $1/k$ at the proper intersection given in the *NACA 685* text, are nearly identical, as seen in the row of Table 3 corresponding to figure 1.

Figure 2. – Figure 2 contains raw form results for Case 2 and also has two real loci and one imaginary locus. In this case, there is no proper intersection, so there is no flutter indicated over this range of $1/k$. The agreement between all original and recomputed loci is excellent. It can be seen that the authors of *NACA 685* stopped performing calculations at values of $1/k$ higher than about 2.25, a reasonable step considering that all calculations were performed by hand and that, with increasing values of $1/k$, the real and imaginary loci were seen to be diverging from each other.

Figure 3. – Figure 3 contains raw form results for Case 3 and again has two real loci and one imaginary locus. Again, there is no proper intersection, so there is no flutter indicated over this range of $1/k$. The agreement between the original and recomputed real loci is excellent. However, for values of $1/k$ above about 0.5, there is a growing difference between the original and recomputed imaginary loci, until, at the highest value of $1/k$ for which original calculations were made, the difference is about 25 percent. This pattern of excellent agreement for the real loci and poor agreement for the imaginary locus will be seen again later in this paper for other Case 3 examples.

Figure 4. – Figure 4 contains raw form results for the 3 DOF flutter problem, and thus, has three real loci and two imaginary loci, clearly seen. Figure 4 has a single proper intersection at a value of $1/k$ near 0.8, producing a single flutter mode. (In the lower-left corner of the figure, at values of $1/k$ near zero and values of $\sqrt{X}$ near one, although the scale and resolution of the plot are not fine enough to distinguish it, the real and imaginary loci in that vicinity, both original and recomputed, do not intersect; each imaginary locus begins above its respective real locus and remains above with increasing values of $1/k$.) The original calculations extend to values of $1/k$ of two; recomputed calculations extend to values of $1/k$ of four, with corresponding extensions (in faint gray) of the original grid. The extension of the recomputed results to higher values of $1/k$ shows that the top two real loci are approaching each other and that one of the imaginary loci has "reappeared" at a value of $1/k$ of about 2.9.

Over the range of $1/k$ from zero to two, the agreement between the original and recomputed loci appears to be excellent. At a cursory inspection, the agreement between the original and recomputed proper intersections also appears to be excellent, which would necessarily mean that the agreement between corresponding flutter velocities and flutter reduced frequencies would also be excellent. However, at closer inspection, this is not the case. As seen in the row of Table 3 corresponding to figure 4, at the proper intersection, although the original and recomputed values of $\sqrt{X}$ are almost identical,

the corresponding values of $1/k$ differ by more than 17 percent, not apparent due to the scale and resolution of the plot.

Equation (10) reveals that flutter velocity is inversely proportional to the product of k_f and $\sqrt{X}$ at the proper intersection, which explains why, for a very small percentage difference in $\sqrt{X}$, the percentage difference between the original and recomputed values of v_f is on the same order as the percentage difference for $1/k$. (The percentage difference for k_f is identical to the percentage difference for $1/k$.)

Figure 5. – Figure 5 contains four examples for Case 2: one example for each combination of the two parameters, $\left(\frac{\omega_\beta}{\omega_h}\right)^2$ and x_β, with two values each. Figure 5(b) corresponds to figure 2, but with a different vertical scale. All parts of the figure appear to show excellent agreement between the original and recomputed results for the real loci. Figure 5(b) also shows excellent agreement between the original and recomputed results for the imaginary locus. The original and recomputed results for the imaginary locus for parts (a), (c), and (d) show the same trends with increasing values of $1/k$, but with varying amounts of difference between the two.

Parts (a), (b), and (d) contain no intersections of loci, so there is no flutter indicated over their respective ranges of $1/k$. Part (c) contains two intersections, indicating two flutter conditions, in this instance, a hump mode. Knowledge that these two intersections together form a hump mode was gained from the check performed using the p-method.

As was the case for figure 4, cursory inspection of the overall good agreement between the original and recomputed real and imaginary loci in figure 5(c) suggests that there would also be good agreement between the respective proper intersections. This is the case for the second proper intersection (the one at the higher value of $1/k$, corresponding to the hump-mode restabilizing condition), but it is far from the case for the first proper intersection (at the lower value of $1/k$, the destabilizing condition).

Table 3 reveals that, at the first proper intersection, the values of $\sqrt{X}$ are identical, but that the values of $1/k$ differ by over 150 percent, which results in comparably large percentage differences in v_f and k_f. (It is a coincidence that the recomputed value of v_f is close to Theodorsen's and Garrick's value of k_f, and vice versa.) This large percentage difference between values of $1/k$ is not apparent because of the scale of the horizontal axis in figure 5(c) and the resolution of the loci. At the second proper intersection, the values of $\sqrt{X}$ are again identical, but the values of $1/k$ differ by less than two and a half percent, resulting in comparable percentage differences in v_f and k_f.

Figure 6. – Figure 6 contains four examples for Case 3: one example for each combination of the two parameters, $\left(\frac{\omega_\beta}{\omega_\alpha}\right)^2$ and x_β, with two values each. (In figure 6, the value $\frac{3}{32}$ for $\left(\frac{\omega_\beta}{\omega_\alpha}\right)^2$ produces the same value of ω_β as does the value $\frac{3}{2}$ for $\left(\frac{\omega_\beta}{\omega_h}\right)^2$ in figure 5.) Figure 6(b) corresponds to figure 3, but with a different vertical scale.

All parts of the figure show excellent agreement between the original and recomputed real loci. With increasing values of $1/k$, all parts of the figure show increasing differences between the original and recomputed imaginary loci. Because of the amount of checking and rechecking of the equations and the Matlab® code for Case 3 (all successful), the present author believes that these differences are due to errors made by the authors of *NACA 685*. Additional evidence supporting this belief appears in the discussion of Graph III-B, later in this paper.

Parts (a) and (b) contain no intersections of loci, so there is no flutter indicated over their ranges of $1/k$. Parts (c) and (d) each contain a pair of intersections, indicating hump-mode flutter for each part (again, confirmed by the p-method). In parts (c) and (d), the first intersection (at lower $1/k$) corresponds to the velocity and reduced frequency of instability; the second intersection (at higher $1/k$) corresponds to the velocity and reduced frequency of regained stability.

In examining the rows of Table 3 corresponding to figures 6(c) and 6(d), one sees that, for each of the four proper intersections, the percentage differences between the original and recomputed values of $1/k$ are all significantly larger than the corresponding percentage differences between the original and recomputed values of $\sqrt{X}$. In addition, the percentage differences between the original and recomputed values of $1/k$ at the two destabilizing conditions (at lower $1/k$) are each larger than their corresponding differences at the two restabilizing conditions (at higher $1/k$). And finally, the percentage differences between the original and recomputed values of $\sqrt{X}$ at the restabilizing conditions are larger than the corresponding differences at the destabilizing conditions because of the increasing differences between the original and recomputed imaginary loci with increasing values of $1/k$.

In terms of a physical interpretation of the results in figure 6, for parts (a) and (b), the quantity x_β is zero, corresponding to the aileron center of gravity colocated with the aileron hinge; for parts (c) and (d), quantity x_β is 0.0066, corresponding to the aileron center of gravity located aft of the hinge. Because parts (a) and (b) are flutter free and parts (c) and (d) are characterized by hump-mode flutter, for this particular "large modern airplane" aileron, mass balancing is required to avoid flutter.

Figure 7. – Figure 7 contains four examples for the 3DOF flutter problem: one example for each combination of the two parameters, $\left(\frac{\omega_\beta}{\omega_h}\right)^2$ and x_β, with two values each. (The four pairs of parameters in figure 7 correspond to the same values of ω_β and x_β as those in figures 5 and 6.) Figure 7(b) corresponds to figure 4, but with a different vertical scale.

All parts of the figure contain intersections of real and imaginary loci: parts (a), (b), and (d) contain a single intersection each, corresponding to a single flutter mode; part (c) contains three intersections, corresponding to a single flutter mode and a hump mode.

With an exception, addressed in the following paragraph, all parts of the figure show good-to-excellent agreement between the original and recomputed real loci and the original and recomputed imaginary

loci. There are areas of the plots where small differences are apparent, but overall, the shapes of the original and recomputed loci match very well.

The exception is the imaginary locus visible in the lower right corners of parts (a), (b), and (c). The recomputed results show fragments of an imaginary locus in all three parts. The original results show a fragment for part (c) only. For parts (a) and (b), the explanation for the missing original imaginary loci could simply be the fact that calculations for the original results were terminated at a value of $1/k$ before these loci would have appeared. If the original results had continued to higher values of $1/k$, the missing loci may have appeared. For part (c), there is a significant difference between the original and recomputed imaginary loci, but it is unknown why.

As was observed in figures 4, 5 and 6, a cursory inspection of the original and recomputed loci that initially suggests good agreement, does not guarantee good agreement of the original and recomputed proper intersections. Closer inspection is required. This is also the case for parts (a), (b), and (d) of figure 7, each of which contains a single proper intersection. The corresponding rows in Table 3 indicate larger percentage differences between the original and recomputed values, for both v_f and k_f, than might initially be assumed by cursory inspection. At these proper intersections, the percentage difference between the original and recomputed values of $1/k$ is always larger (in one case more than an order of magnitude larger) than the corresponding percentage difference between the original and recomputed values of $\sqrt{X}$.

Figure 7(c) contains three proper intersections. The two proper intersections in the upper left portion of the figure correspond to a hump mode. The proper intersection at the lower value of the inverse of reduced frequency corresponds to the destabilizing condition; the one at the higher value, the restabilizing condition. The appropriate rows in Table 3 reveal that, as has been seen previously, there is a significantly larger percentage difference between the values of $1/k$ at the destabilizing condition than there is at the restabilizing condition, causing large percentage differences in both v_f and k_f.

The proper intersection at the bottom of the figure corresponds to a single flutter mode. Percentage differences in v_f and k_f for this single flutter mode are consistent with the percentage differences for the single flutter modes in parts (a), (b), and (d).

Comparing original figure 4 and original figure 7(b). – It was stated above that figure 7(b) corresponds to figure 4, meaning that the same physical constants were used to produce each figure. That tabular results have been given for each presents an opportunity to determine if the results in *NACA 685* are self-consistent. The following table collects the original results from Table 3 and compares the proper intersections and flutter results:

	Proper Intersection		Flutter Condition	
	$1/k$	$\sqrt{X}$	v_f, fps	k_f
Original Fig. 4	0.875	1.060	445.8	1.143
Original Fig. 7(b)	0.852	1.121	410.7	1.173
% Difference	2.7	5.6	8.3	2.7

These results should be identical, but there are nontrivial differences. If one assumes that the same original computations were used to produce the original real and imaginary loci in each figure, then the percentage differences in v_f and k_f revealed in this table can be attributed to one of two causes:

(1) inconsistencies in hand-plotting from figure to figure resulting in differences in the proper intersections in the two figures;
(2) human error in reading the values of $1/k$ and $\sqrt{X}$ in figure 4 (by the authors of *NACA 685*), human error in reading the values of $1/k$ and $\sqrt{X}$ in figure 7(b) (by the present author), or both.

Regardless of the reason for the differences in v_f and k_f, that these differences exist emphasizes that the potential for error was always present at a time when humans performed tasks that are now performed routinely by computers. These differences also offer their own justification, independent of Zeiler's (ref. 1) justification, for recomputing all the example problems in *NACA 685*: If the flutter velocities predicted by two raw-form renditions of the same problem differ by 8.3 percent, can there be confidence in any prediction of flutter velocity in *NACA 685*?

Observations. – Table 3 summarizes the 14 flutter conditions obtained from the proper intersections in the raw form illustrations of the *NACA 685* solution method contained in figures 1, 4, 5, 6, and 7. This table reveals two related results regarding the value of $1/k$ at proper intersections:

(1) In the four instances of hump modes, for both original and recomputed results, the value of $1/k$ at the destabilizing condition is always less than that at the restabilizing condition. In addition, the percentage difference between the original and recomputed values of $1/k$ at the destabilizing condition is always larger than that at the restabilizing condition.
(2) For both single flutter modes and hump modes, there are six instances (including the destabilizing condition for all hump modes) in which the value of $1/k$ (original and recomputed) is below 0.5; for these six, the average percentage difference between the original and recomputed values of $1/k$ is 61.3. There are eight instances (including the destabilizing condition for all hump modes) in which the value of $1/k$ (original and recomputed) is above 0.5; for these eight, the average percentage difference between the original and recomputed values of $1/k$ is 11.4.

For these flutter conditions, there is an approximate inverse relationship between the original value of $1/k$ at the proper intersection and the corresponding percentage difference between the original and recomputed values of $1/k$ at the proper intersection: when one is low, the

other is high. The reason for this is unknown, but perhaps Theodorsen and Garrick could have achieved more accurate results (and thereby lowered the percentage differences in $1/k$) had they solved their equations at more values of $1/k$ between zero and 0.5.

Flutter Solutions for Variations in Frequency Ratio

Figures 8, 17, 19, and 26 each contain plots representing multiple flutter solutions: figures 8, 17, and 26 contain plots of flutter velocity (in normalized form in fig. 8) as a function of the ratio of modal frequencies; figure 19 contains normalized flutter frequency as a function of the ratio of modal frequencies and is a companion to figure 17. Figure 8 is for the 3DOF flutter problem; figures 17 and 19 are for Case 1; figure 26 is for Case 2. Figures 17, 19, and 26 also contain experimental results.

The original results are shown as continuous curves, created by the authors of *NACA 685* by fairing through a discrete number of points, each discrete point representing a single execution of the *NACA 685* solution method. It is not known how many individual executions of the solution method were performed by the authors to produce the original continuous curves.

Each colored symbol in these figures (that is, each recomputed result) represents a single execution of the solution method, with flutter velocities and flutter reduced frequencies determined from proper intersections.

Figure 8. – Figure 8 corresponds to the 3DOF flutter problem. The ordinate in figure 8 is normalized flutter velocity (referred to in *NACA 685* as "flutter-speed coefficient") and the abscissa is the ratio of frequencies, $\frac{\omega_\beta}{\omega_\alpha}$. The black curve and colored circle symbols correspond to the original and recomputed results, respectively. Each colored circle symbol represents a single solution of the 3DOF flutter problem. There are three points to be made about this figure.

First, for the original and recomputed results, the overall behaviors of the normalized flutter velocity with increasing modal-frequency ratio are very similar, but there are noticeable differences, the largest occurring at $\frac{\omega_\beta}{\omega_\alpha} = 0.4$, where the difference between the two results is on the order of 20%.

Second, the asymptotic value of normalized flutter velocity, 1.54, indicated top right in the figure, corresponds to the frequency ratio, $\frac{\omega_\beta}{\omega_\alpha}$, becoming infinitely large. At an infinitely large value of $\frac{\omega_\beta}{\omega_\alpha}$, the 3DOF flutter problem approaches the 2DOF flutter problem of Case 1 (involving h and α). Recomputed calculations for the 3DOF flutter problem for $\frac{\omega_\beta}{\omega_\alpha} = 1\text{x}10^5$ (for this example, a value sufficiently large to be considered "infinitely large") produced a value of normalized flutter velocity of 1.545, confirming the result shown in figure 8. The corresponding recomputed value of normalized flutter velocity for the 2DOF flutter problem is also 1.545.

Third, the solution at $\frac{\omega_\beta}{\omega_\alpha} = 0$ in figure 8 corresponds to the solution depicted in figure 7(a). This fact offers another opportunity to check the self-consistency of results in *NACA 685*. In figure 8, at $\frac{\omega_\beta}{\omega_\alpha} = 0$,

the present author determined the value of $\frac{v}{b\omega_\alpha}$ to be 0.698. Knowing, from Table 2, that the product $b\omega_\alpha$ is 540, this value of $\frac{v}{b\omega_\alpha}$ corresponds to a flutter velocity of 376.9 feet per second. As determined from reading the values of $1/k$ and $\sqrt{X}$ at the proper intersection in figure 7(a), Table 3 lists the "original" flutter velocity as 387.5 feet per second. Thus, there is a 2.8% difference between these two original values of flutter velocity.

Figures 17 and 19. – Figures 17 and 19 are companion figures, the former presenting flutter velocity in miles per hour as a function of the frequency ratio $\frac{\omega_h}{\omega_\alpha}$, the latter presenting flutter frequency normalized by the torsion frequency, also as a function of the frequency ratio $\frac{\omega_h}{\omega_\alpha}$. These figures correspond to Case 1 (involving h and α). (Experimental data for wings 2A, 2B, 3 and 4, whose characteristics are identified in *NACA 685*, is also included in both figures.) The agreement between the original and the recomputed results in both figures is excellent (as is the agreement between the original and the experimental results).

Figure 26. – Figure 26 contains two examples for Case 2 (involving β and h) and illustrates the effect of structural damping on the flutter velocity. The ordinate is flutter velocity in miles per hour and the abscissa is the modal-frequency ratio, $\frac{\omega_\beta}{\omega_h}$. The key in the center of the figure identifies which set of recomputed theoretical results corresponds to which set of original theoretical results: the solid theoretical line and the blue circles correspond to structural damping absent from both modes (g_h=g_β= 0); the dashed theoretical line and the red circles correspond to structural damping absent from the aileron mode (g_β= 0), but present in the flexure mode (g_h= 0.0125). Also present in the figure are experimental results corresponding to wing 5 with aileron AII. Experimental data are indicated by the cross-hatched area and open black circles.

All flutter results in figure 26 are hump modes, characterized in this figure by two flutter velocities at the same value of $\frac{\omega_\beta}{\omega_h}$. The lower velocity is the destabilizing velocity; the upper velocity is the restabilizing velocity. Between these velocities the configuration is unstable; below and above these velocities the configuration is stable.

The original and the recomputed results show fair-to-good agreement in some areas of the figure and excellent agreement in other areas. In both sets of results, an increase in the value of $\frac{\omega_\beta}{\omega_h}$ to a large enough value causes the hump mode to disappear completely, and the disappearance happens more quickly (i.e., at lower values of $\frac{\omega_\beta}{\omega_h}$) for the case with structural damping than for the case without.

The original results for both combinations of structural damping conditions miss the pronounced dips (at $\frac{\omega_\beta}{\omega_h}$ =0.4 for the blue dots, at $\frac{\omega_\beta}{\omega_h} = 0.8$ for the red dots) that characterize recomputed results for the destabilizing velocities. These misses could be attributed to the authors of *NACA 685* performing relatively few calculations (at least fewer than the recomputed calculations), thus fairing their curves through the sparser number of points, and thereby missing this key variation in the quantity of interest.

Both the original results and the recomputed results show that the inclusion of structural damping reduces the respective regions of instability. For both sets of results with structural damping present, across the entire range of frequency ratio, flutter onset occurs at higher velocities and regaining stability occurs at lower velocities.

Observations. – In figures 8, 17, 19, and 26, with increasing values of frequency ratio, the original and recomputed results show the same trends and the agreement between them ranged from good to excellent. The original results in figures 8 and 26 did not include knowledge of flutter reduced frequency and, for this reason, it was impossible to discern whether differences between original and recomputed flutter velocities were due to differences in $1/k$ at proper intersections, differences in $\sqrt{X}$ at proper intersections, or both.

VIII. RECOMPUTATION AND COMPARISON OF RESULTS CONTAINED IN GRAPHS OF *NACA 685*

The graphs contain the vast majority of the theoretical results in *NACA 685* in the form of dozens of parametric variations. Many graphs have multiple parts. The recomputations for the graphs required on the order of 2000 individual executions of the *NACA 685* solution method.

Preliminaries

The following information is intended as an aid in understanding the results (original and recomputed) contained in the graphs of *NACA 685*.

Arrangement. – There are 16 graphs, each identified by a Roman numeral and a capital letter, hyphenated. All graphs are for 2DOF flutter problems: graphs I-A through I-G contain results solely for Case 1; graphs II-A through II-F, Case 2; and graphs III-A through III-C, Case 3.

Ordinates and abscissas in graphs. – In the graphs, the authors of *NACA 685* introduce Case-specific flutter-speed coefficients (identified as $\frac{v}{b\omega_\alpha}$ for Cases 1 and 3, and as $\frac{v}{b\omega_h}$ for Case 2) that are used as the ordinates of all graphs except one. The exception is graph I-F, which has as its ordinate normalized flutter frequency, $\frac{\omega_f}{\omega_\alpha}$. The authors of *NACA 685* use the ratio of natural frequencies ($\frac{\omega_h}{\omega_\alpha}$, $\frac{\omega_\beta}{\omega_h}$, and $\frac{\omega_\beta}{\omega_\alpha}$ for Cases 1, 2, and 3, respectively) as the abscissa for many of the graphs.

For the remainder of this paper, the term “normalized flutter velocity” will be used instead of “flutter-speed coefficient.” In addition, in order not to lose sight of the fact that $\frac{v}{b\omega_\alpha}$ and $\frac{v}{b\omega_h}$ refer to flutter conditions, in the present paper, subscript f will be added to the velocity in these expressions, becoming $\frac{v_f}{b\omega_\alpha}$ and $\frac{v_f}{b\omega_h}$, respectively.

Parametric variations. – Of the physical constants required to uniquely define a given configuration (a, b, c, κ, x_α, r_α^2, x_β, r_β^2, ω_α, ω_β, ω_h, g_α, g_β, g_h, and ξ), all except b and ω_α are used as parameters in the graphs and more than half of the physical constants are used as parameters in two or more graphs.

Elimination of some values of parameters in recomputations. – A single part of a single graph may contain up to six original curves, with each curve representing one value of a parameter. Because of the sheer number of recomputations that would have been required to duplicate each original curve in each part of each graph, in some instances, not all values of the parameter were chosen for the recomputations. In those instances, a representative subset of values was chosen.

Interpretation of symbols in graphs. – Recomputed results are shown as colored symbols. If a symbol is present, flutter is present. There are some instances when, at the next increment of the independent variable, flutter is no longer present. In these instances, the last symbol for which flutter is present is given a bold black outline to alert the reader that there is no flutter beyond that value.

Graphs for Case 1

Graphs I-A through I-G contain 2DOF examples for Case 1 (involving h and α).

Graph I-A. – Graph I-A shows the effect of increasing values of frequency ratio, $\frac{\omega_h}{\omega_\alpha}$, on normalized flutter velocity, $\frac{v_f}{b\omega_\alpha}$, with x_α, the distance between the elastic axis and the center of gravity of the entire wing, as the parameter. Recomputations were performed for a subset of values of the parameter.

Graph I-A uses the following physical constants as –

– discrete values: $b = 6$; $r_\alpha^2 = \frac{1}{4}$; $\omega_\alpha = 90$; $g_\alpha = 0$; $g_h = 0$; $\xi = 1$

– ranges of values: $\kappa = \frac{1}{20}, \frac{1}{10}, \frac{1}{5}, \frac{1}{4}, \frac{1}{3}, \frac{1}{2}$; $a = -0.2, -0.3, -0.4, -0.45$.

Because of the many possible combinations of κ and a graph I-A contains 26 parts, (a) through (u). Table 4 shows the arrangement of these combinations within graph I-A.

The agreement between the original and recomputed results in graph I-A ranges from excellent in some places to poor in others.

In all parts of the graph (that is, over the entire ranges of κ and a and for all values of x_α), up to values of $\frac{\omega_h}{\omega_\alpha}$ of about 0.8, there is good-to-excellent agreement between the original and recomputed results, including the mutual crossings of the red, blue, and green curves in parts (k) and (m) through (u).

Above values of $\frac{\omega_h}{\omega_\alpha}$ of about 0.8, some of the curves continue to display good-to-excellent agreement, but in many instances the original and recomputed results differ significantly. One common difference between the original and recomputed results is illustrated by the blue results ($x_\alpha = 0.2$) in part (l) and the red results ($x_\alpha = 0.1$) in part (n): with increasing values of $\frac{\omega_h}{\omega_\alpha}$ both sets of results reach a minimum

and then increase, but in the vicinity of their respective minima the recomputed results display much steeper slopes (negative and positive) than do the original results. Another common difference between the original and recomputed results is illustrated by the blue results ($x_\alpha = 0.2$) in part (j) and the red results ($x_\alpha = 0.1$) in part (l): with increasing values of $\frac{\omega_h}{\omega_\alpha}$ the original results reach a minimum and then increase, but (at least over the range of $\frac{\omega_h}{\omega_\alpha}$ shown) the recomputed results continue to decrease.

It should be acknowledged that in reference 1 Zeiler chose part (q) of Graph I-A (as reproduced from ref. 6) to illustrate the differences between the original results and his results. Appendix B of the present paper contains comparisons of Zeiler's results and present recomputed results.

Graph I-B. – Graph I-B shows the effect of increasing the distance from the midchord to the center of gravity of the entire wing, the sum $(a + x_\alpha)$, on normalized flutter velocity, $\frac{v_f}{b\omega_\alpha}$. Quantity a is the distance from the midchord to the elastic axis and quantity x_α is the distance from the elastic axis to the center of gravity, both measured positive aft. Quantity a is the parameter. In part (b), recomputations were performed for a subset of values of the parameter.

Graph I-B uses the following physical constants as –

– discrete values: $\kappa = \frac{1}{10}; b = 6; r_\alpha^2 = \frac{1}{4}; \omega_\alpha = 90; g_\alpha = 0; g_h = 0; \xi = 1$

– ranges of values: $\left(\frac{\omega_h}{\omega_\alpha}\right)^2 = 0,\ \frac{1}{2}$.

The agreement between the original and recomputed results in graph I-B is good-to-excellent. The square of the frequency ratio for part (a) is zero and for part (b) is $\frac{1}{2}$; otherwise all physical constants in both parts are identical. In part (a), the results collapse approximately to a single curve, which *NACA 685* points out, "… shows clearly that the value of a actually has no influence on the flutter speed." In part (b), it is seen that the parametric curves are spread horizontally over the extent of the plot, indicating the effect of a on flutter speed.

Graph I-C. – Graph I-C shows the effect of increasing the inverse of the mass ratio, $\frac{1}{\kappa}$, on normalized flutter velocity, $\frac{v_f}{b\omega_\alpha}$, with x_α, the distance between the elastic axis and the center of gravity of the entire wing, as the parameter. Recomputations were performed for a subset of values of the parameter. No recomputations were performed for part (j).

Graph I-C uses the following physical constants as –

– discrete values: $b = 6; r_\alpha^2 = \frac{1}{4}; \omega_\alpha = 90; g_\alpha = 0; g_h = 0; \xi = 1$

– ranges of values: $\left(\frac{\omega_h}{\omega_\alpha}\right)^2 = 0, \frac{1}{10}, \frac{1}{2};\ a = -0.2, -0.3, -0.4.$

The authors of *NACA 685* chose as the abscissa the inverse of mass ratio, $\frac{1}{\kappa}$, which, according to the definition of κ in the Section II, is equal to $\frac{M}{\pi\rho b^2}$. Therefore, for a given configuration at a given air density, moving to the right along the abscissa corresponds to increasing wing mass, while moving to the left corresponds to decreasing wing mass. So, one way to understand the results in this graph is to proceed along the abscissa from right to left, interpreting the various curves to reveal the effect of decreasing wing mass on the flutter velocity. The discussion below interprets the curves in this way.

In reviewing all parts of the graph, the original and recomputed results are seen to have the same trend: reductions in nondimensional flutter velocity (some more shallow or more steep than others), some with and some without an up-tick at the lowest values of mass (depending on the particular values of $\left(\frac{\omega_h}{\omega_\alpha}\right)^2$ and a).

For all parts of this graph except part (g), agreement between the original and recomputed results is good-to-excellent. However, in part (g), there is significant discrepancy between the original and recomputed results for $x_\alpha = 0$.

There are five instances in the graph ($x_\alpha = 0$ in parts (d), (e), (g), (h) and $x_\alpha = 0.05$ in part (g)) in which the recomputed results predict flutter ceasing at a higher mass than the original results do, as indicated by the symbols with the bold outlines.

It should be acknowledged that, in reference 1, Zeiler chose part (h) of this graph (also reproduced from ref. 6, where the abscissa has been extended to a value of 100) to illustrate the differences between the original results and his results. Appendix B of the present paper also contains comparisons of Zeiler's results and present recomputed for this part of Graph I-C.

Graph I-D. – Graph I-D shows the effect of increasing values of frequency ratio, $\frac{\omega_h}{\omega_\alpha}$, on normalized flutter velocity, $\frac{v_f}{b\omega_\alpha}$, for various combinations of structural damping coefficients, g_α and g_h.

Graph I-D uses the following physical constants as –

– discrete values: $a = -0.2; b = 6; \kappa = \frac{1}{10}; x_\alpha = 0.1; r_\alpha^2 = \frac{1}{4}; \omega_\alpha = 90; \xi = 1.$

Of note in the graph are the following:

(1) The condition $g_h = g_\alpha = 0$ is present in part (a) and is repeated in parts (b) and (c). The gray curves and gray solid circles represent this condition in all three parts of the graph;
(2) The condition $g_h = g_\alpha = 0.1$ is present in part (a) and is repeated in part (b). The blue curves and blue solid circles represent this condition in parts (a) and (b);
(3) The condition $g_h = g_\alpha = 0.2$ is present in part (a) and is repeated in part (c). The green curves and green solid circles represent this condition in parts (a) and (c).

All parts of the graph show good-to-excellent agreement between the original and recomputed results up to a point. A notable difference is that in several instances the recomputed results show flutter terminating at various values of $\frac{\omega_h}{\omega_\alpha}$ (indicated by bold outlines around various symbols) while the original results show flutter continuing past these values of $\frac{\omega_h}{\omega_\alpha}$, and in some instances well past. In part (a), in which g_α and g_h are assigned identical values in each parametric variation, it can be seen that at each value of frequency ratio increasing the value of structural damping increases the flutter velocity. From parts (b) and (c), it can be seen that at lower values of frequency ratio, g_α alone is more effective than g_h alone in increasing the flutter velocity, but at higher values of frequency ratio the opposite is true.

Graph I-E. – Graph I-E shows the effect of increasing values of frequency ratio, $\frac{\omega_h}{\omega_\alpha}$, on normalized flutter velocity, $\frac{v_f}{b\omega_\alpha}$, with r_α^2, the square of the nondimensional radius of gyration about the elastic axis, as the parameter.

Graph I-E uses the following physical constants as –

– discrete values: $a = -0.2;\ b = 6;\ x_\alpha = 0.1;\ \omega_\alpha = 90;\ g_\alpha = 0;\ g_h = 0;\ \xi = 1$

– ranges of values: $\kappa = \frac{1}{20}, \frac{1}{10}, \frac{1}{5}$.

Portions of all parts of the graph show good-to-excellent agreement between the original and recomputed results. But in each portion, for frequency ratios greater than about unity, the original and recomputed results sometimes deviate substantially from each other. One notable difference is that in part (a), for all curves except $r_\alpha^2 = 1$, the recomputed results show flutter terminating at various values of $\frac{\omega_h}{\omega_\alpha}$ while the original results show flutter velocity increasing and continuing past these values of $\frac{\omega_h}{\omega_\alpha}$.

Graph I-F. – Graph I-F shows the effect of increasing values of frequency ratio, $\frac{\omega_h}{\omega_\alpha}$, on nondimensional flutter frequency, $\frac{\omega_f}{\omega_\alpha}$, with x_α, the distance between the elastic axis and the center of gravity of the entire wing, as the parameter. Parts (a), (b), (c), and (d) in this graph contain companion information to parts (j), (l), (m), and (o), respectively, of graph I-A. Recomputations were performed for a subset of values of the parameter.

Graph I-F uses the following physical constants as –

– discrete values: $b = 6;\ r_\alpha^2 = \frac{1}{4};\ \omega_\alpha = 90;\ g_\alpha = 0;\ g_h = 0;\ \xi = 1$

– ranges of values: $\kappa = \frac{1}{10}, \frac{1}{5};\ a = -0.2, -0.4.$

In all parts of the graph, the original and recomputed results follow the same trends with increasing values of frequency ratio, $\frac{\omega_h}{\omega_\alpha}$, including, for the red and gray curves and symbols in part (d), displaying the identical inflections. In all parts of the figure, there are areas of excellent agreement between the original and recomputed results: this is true for all blue and red curves and symbols and for most gray

curves and symbols at $\frac{\omega_h}{\omega_\alpha} = 0$; this is also true for all blue and red curves and symbols for values of $\frac{\omega_h}{\omega_\alpha}$ at and above 0.7; and this is again true for gray curves and symbols in parts (a), (c), and (d) for the same range in $\frac{\omega_h}{\omega_\alpha}$. However, in all parts of the figure over the range of $\frac{\omega_h}{\omega_\alpha}$ between 0.1 and 0.6, the agreement between the original and recomputed results is only good to fair, with the most prominent disagreements at $\frac{\omega_h}{\omega_\alpha} = 0.3$.

Graph I-G. – Graph I-G shows the effect of increasing values of frequency ratio, $\frac{\omega_h}{\omega_\alpha}$, on normalized flutter velocity, $\frac{v_f}{b\omega_\alpha}$, with the modal coupling factor, ξ, as the parameter.

Graph I-G uses the following physical constants as –

– discrete values: $a = -0.2;\ b = 6;\ \kappa = \frac{1}{10};\ x_\alpha = 0.2;\ r_\alpha^2 = \frac{1}{4};\ \omega_\alpha = 90;\ g_\alpha = 0;\ g_h = 0.$

For a modal coupling factor of unity, the character of the original and recomputed results is the same, with excellent agreement up to a value of frequency ratio of about 1.0, but with increasing disagreement as frequency ratio increased beyond 1.0. At the highest frequency ratio, the difference is about 30%.

For modal coupling factors less than unity, the characters of the original and recomputed results agree very well in some areas but differ significantly in other areas. The recomputed results show hump modes over their entire respective ranges of frequency ratio. The original results show hump modes for only the higher portions of their respective ranges of frequency ratio.

For modal coupling factors less than unity, the portions of the original and recomputed results corresponding to the destabilizing velocities of the recomputed hump modes show excellent agreement up to frequency ratios of 0.7 (for $\xi = ⅜$), 0.8 (for $\xi = ½$), and 1.1 (for $\xi = ¾$). Beyond those values of frequency ratio, the agreement between the original and recomputed results breaks down. It is not known why the original results miss the full extents of their hump modes.

Observations. – The graphs for Case 1 contain multiple parametric variations. The original and recomputed results generally show the same trends with increases or decreases in the value of the parameter. The single exception to this is in Graph I-G where the characteristics of the original and recomputed hump modes are drastically different. In those graphs whose abscissa is the frequency ratio $\frac{\omega_h}{\omega_\alpha}$, the agreement between the original and recomputed results is generally better at the lower values of $\frac{\omega_h}{\omega_\alpha}$ than it is at the higher values.

Graphs for Case 2

Graphs II-A through II-F contain 2DOF examples for Case 2 (involving β and h).

Graph II-A. – Graph II-A shows the effect of increasing values of frequency ratio, $\frac{\omega_\beta}{\omega_h}$, on normalized flutter velocity, $\frac{v_f}{b\omega_h}$, for three different parameter variations: parts (a) and (b) have x_β as the parameter; part (c) has g_β and g_h as parameters; and part (d) has r_β^2 as the parameter. For all parts of the graph, $b = 6$, $c = \frac{1}{2}$, $\omega_h = 22.5$, and $\xi = 1$. Discrete values and ranges of values of the other physical constants are indicated in the legend for each part of the graph.

In all parts of the graph, the original results and the recomputed results indicate hump modes over the ranges of the independent variables. And, except for part (b), the original and recomputed results show good-to-excellent agreement. Part (b) shows significant disagreement between the magnitudes of normalized flutter velocities, especially for $x_\beta = \frac{1}{30}$. The disagreements for part (b) are addressed in the next paragraph.

Part (b) presents results for parametric variations in x_β for a constant value of r_β^2; part (d) presents results for parametric variations in r_β^2 for a constant value of x_β. All other physical constants are identical for parts (b) and (d) ($b = 6$, $c = \frac{1}{2}$, $\kappa = \frac{1}{10}$, $\omega_h = 22.5$, $g_\beta = 0$, $g_h = 0$, and $\xi = 1$).

One set of results in part (b) shares identical physical constants with a set of results in part (d) ($x_\beta = \frac{1}{60}$ and $r_\beta^2 = \frac{1}{120}$,) and coincidentally, both sets are represented in their respective parts by red curves and symbols. Therefore, one would expect that the original results in parts (b) and (d) would be identical to each other as would the corresponding recomputed results. This is the case for the recomputed results (the red symbols in each part have identical values at corresponding values of frequency ratio), but this is not the case for the original results (the red curves display noticeably different values). This difference in original values between parts (b) and (d), coupled with the good-to-excellent agreement between the original and recomputed in all other parts of the graph and successful checks of the recomputed results using the p-method of flutter solution, suggests that all original results in part (b) are in error.

Graph II-B. – Graph II-B shows the effect of increasing values of x_β, the distance between the aileron hinge and the center of gravity of the aileron, on normalized flutter velocity, $\frac{v_f}{b\omega_h}$, with the square of the ratio of natural frequencies, $\left(\frac{\omega_\beta}{\omega_h}\right)^2$, as the parameter.

Graph II-B uses the following physical constants as –

– discrete values: $b = 6$; $\omega_h = 22.5$; $g_\beta = 0$; $g_h = 0$; $\xi = 1$

– ranges of values: $c = \frac{1}{2}, \frac{2}{3}$; $\kappa = \frac{1}{10}, \frac{1}{5}$; $r_\beta^2 = \frac{1}{500}, \frac{1}{120}, \frac{1}{60}$.

The shapes of the curves in this graph describe hump modes whose restabilizing velocities become increasingly larger as the value of x_β increases. All parts of the graph show good-to-excellent agreement between the original and recomputed results for the destabilizing velocity. Parts (c) and (d) also show good-to-excellent agreement between the original and recomputed results for the

restabilizing velocity. However, for each value of $\left(\frac{\omega_\beta}{\omega_h}\right)^2$ in parts (a) and (b), there are significant differences between the restabilizing velocities for original and recomputed results: in part (a) the recomputed results indicate no restabilizing beyond $x_\beta = 0.04$ and in part (b) the recomputed results indicate no restabilizing beyond $x_\beta = 0.035$; the original results indicate restabilizing beyond.

Graph II-C. – Graph II-C shows the effect of increasing values of r_β^2, the square of the nondimensional radius of gyration of the aileron about the aileron hinge, on normalized flutter velocity, $\frac{v_f}{b\omega_h}$, for four values of $\left(\frac{\omega_\beta}{\omega_h}\right)^2$.

Graph II-C uses the following physical constants as –

– discrete values: $b = 6$; $c = \frac{1}{2}$; $\kappa = \frac{1}{10}$; $x_\beta = \frac{1}{60}$; $\omega_h = 22.5$; $g_\beta = 0$; $g_h = 0$; $\xi = 1$.

The original and recomputed results show fair-to-excellent agreement. The recomputed results and some of the original results indicate hump modes for each value of $\left(\frac{\omega_\beta}{\omega_h}\right)^2$, but the original results omit from the graph the destabilizing flutter velocities for $\left(\frac{\omega_\beta}{\omega_h}\right)^2 = 0$ and $\left(\frac{\omega_\beta}{\omega_h}\right)^2 = \frac{1}{2}$. Progressing to the right in the graph, the lower curves all originate from the same value of $\frac{v_f}{b\omega_h}$, as the upper curves all originate from a different value of $\frac{v_f}{b\omega_h}$. No indication is given in *NACA 685* as to why the two lower curves were omitted.

Graph II-D. – Graph II-D shows the effect of increasing values of frequency ratio, $\frac{\omega_\beta}{\omega_h}$, on normalized flutter velocity, $\frac{v_f}{b\omega_h}$, with x_β, g_β, and g_h as parameters.

Graph II-D uses the following physical constants as –

– discrete values: $b = 6$; $c = 0$; $r_\beta^2 = \frac{1}{20}$; $\omega_h = 22.5$; $\xi = 1$

– ranges of values: $\kappa = \frac{1}{5}, \frac{1}{2}$; $x_\beta = \frac{1}{20}, \frac{1}{10}$.

In all parts of the graph (except part (d)), the original results and the recomputed results indicate hump modes over the ranges of the independent variable. Parts (a) and (b) show good-to-excellent agreement between the original and recomputed results. In part (c), the comparisons for $g_\beta = g_h = 0$ are good-to-excellent, but comparisons for $g_\beta = g_h = 0.2$ show differences over 30 percent. In part (d), the comparisons for $g_\beta = g_h = 0$ are good-to-excellent, but the original results for $g_\beta = g_h = 0.018$ indicate only a single instability at $\frac{\omega_\beta}{\omega_h} = 0$, completely missing the hump-mode nature of the instability indicated by the recomputed results.

Graph II-E. – Graph II-E shows the effect of increasing values of x_β, the distance between the aileron hinge and the center of gravity of the aileron, on normalized flutter velocity, $\frac{v_f}{b\omega_h}$, with $\left(\frac{\omega_\beta}{\omega_h}\right)^2$, g_β, and g_h as parameters.

Graph II-E uses the following physical constants as –

– discrete values: $b = 6; c = 0;\ \omega_h = 22.5; \xi = 1$

– ranges of values: $\kappa = \frac{1}{10}, \frac{1}{5};\ r_\beta^2 = \frac{1}{20}, \frac{1}{10}; g_\beta = 0, 0.2; g_h = 0, 0.2.$

This graph is very similar to graph II-B. The only differences are due to the values chosen for some the physical constants. The shapes of the curves in this graph also describe hump modes whose restabilizing velocities become increasingly larger as the value of x_β increases. As with graph II-B, all parts of this graph show good-to-excellent agreement between the original and recomputed results for the destabilizing velocity. Parts (b) and (d) generally show good-to-excellent agreement between the original and recomputed results for the restabilizing velocity (the exception being the green curves and symbols in part (b)). However, as with graph II-B, for each value of $\left(\frac{\omega_\beta}{\omega_h}\right)^2$ in parts (a) and (c), there are significant differences between the restabilizing velocities for original and recomputed results: in part (a) the recomputed results indicate no restabilizing beyond $x_\beta = 0.12$ and in part (c) the recomputed results indicate no restabilizing beyond $x_\beta = 0.1$; the original results indicate restabilizing beyond.

There are two instances in this graph of the same result appearing in part (a) and in part (b): the gray curves and symbols in each part correspond to each other, as do the blue curves and symbols. The gray symbols in each part are identical to each other; the blue symbols in each part are identical to each other. However, if one looks closely at the gray curve in part (a) and the gray curve in part (b) one can discern differences; the same can be said of the blue curve in part (a) and the blue curve in part (b). These differences are speculated to be due to human error in plotting and faring the points that make up the gray and blue curves.

Graph II-F. – Graph II-F shows the effect of increasing values of frequency ratio, $\frac{\omega_\beta}{\omega_h}$, on normalized flutter velocity, $\frac{v_f}{b\omega_h}$, with the modal coupling factor, ξ, as the parameter.

Graph II-F uses the following physical constants as –

– discrete values: $b = 6; c = 0; \kappa = \frac{1}{5}; r_\beta^2 = \frac{1}{6}; x_\beta = \frac{1}{4}; \omega_h = 22.5; g_\beta = 0; g_h = 0.$

Graph II-F is similar to graph I-G, but unlike graph I-G, in which the original and recomputed results differed in character, in graph II-F the character of the curves agrees for each value of modal coupling factor. The agreement between the original and recomputed results is good-to-excellent in all areas of the plot.

Observations. – The graphs for Case 2 also contain multiple parametric variations, but far fewer than those for Case 1. Except for two curves in Graph II-F, the original and recomputed results are all hump

modes and always show the same trends with increases or decreases in the value of the parameter. With a few exceptions (part (b) of Graph II-A and parts (c) and (d) of Graph II-D), the magnitudes of the original and recomputed results are in good-to-excellent agreement with each other.

Graphs for Case 3

Graphs III-A through III-C contain 2DOF examples for Case 3 (involving α and β).

Graph III-A. – Graph III-A shows the effect of increasing values of frequency ratio, $\frac{\omega_\beta}{\omega_\alpha}$, on normalized flutter velocity, $\frac{v_f}{b\omega_\alpha}$, for structural damping absent and structural damping present.

Graph III-A uses the following physical constants as –

– discrete values: $a = -0.4;\ b = 6;\ c = 0.5;\ \kappa = \frac{1}{10};\ x_\beta = \frac{1}{80};\ r_\alpha^2 = \frac{1}{4};\ r_\beta^2 = \frac{1}{160}\ \omega_\alpha = 90;\ \xi = 1.$

The original results and the recomputed results indicate hump modes over the ranges of the independent variable, and except for one region of the zero-structural-damping results, the agreement between the original and recomputed results is good-to-excellent. For all values of frequency ratio, the effect of increasing structural damping from zero (gray curve and symbols) to 0.2 (red curve and symbols) is to minimize the velocity range of the hump mode by increasing the lower flutter velocity and decreasing the restabilizing velocity.

Graph III-B. – Graph III-B shows the effect of increasing values of frequency ratio, $\frac{\omega_\beta}{\omega_\alpha}$, on normalized flutter velocity, $\frac{v_f}{b\omega_\alpha}$, for two values of x_β, the distance from the aileron hinge to the aileron center of gravity.

Graph III-B uses the following physical constants as –

– discrete values: $a = -0.4;\ b = 6;\ c = 0.6;\ \kappa = \frac{1}{4};\ r_\alpha^2 = \frac{1}{4};\ r_\beta^2 = 0.0012;\ \omega_\alpha = 90;$
$g_\alpha = 0;\ g_\beta = 0;\ \xi = 1.$

For both values of x_β, the original results indicate a hump mode, with the lower value of x_β predicting a much smaller region of instability than the higher value predicted. For the recomputed results, a hump mode was predicted for the higher value of x_β, but no instability was predicted for the lower value. For the higher value of x_β, the original and recomputed results show good-to-excellent agreement.

NACA 685 makes no mention of this in its discussion of Graph III-B, but the values of the physical constants used to produce the curve labeled "$x_\beta = 0.0066$" in Graph III-B are identical to those used to produce parts (c) and (d) of figure 6. The values of $\frac{\omega_\beta}{\omega_\alpha}$ in parts (c) and (d) (zero and 0.3062, respectively) are within the range of values of $\frac{\omega_\beta}{\omega_\alpha}$ on the horizontal axis in Graph III-B, making it

possible for the flutter velocities from parts (c) and (d) (indicated in Table 3) to be normalized and plotted on Graph III-B, thereby offering a final self-consistency check on the original results of *NACA-685*. If the original computations in figure 6 and Graph III-B are each correct, the results from parts (c) and (d) of figure 6 should fall exactly on the curve labeled "$x_\beta = 0.0066$" in Graph III-B.

These normalized flutter velocities from parts (c) and (d) of figure 6 appear as the "**x**" and "**+**" symbols in Graph III-B and are seen to be nowhere near falling on the curve labeled "$x_\beta = 0.0066$." In fact, employing the criteria for qualitative assessment of agreement (defined in Table 1 for the agreement between the original and recomputed results, but applying these criteria now to the agreement between the original results from figure 6 and the original results from Graph III-B) one sees that the agreement is only fair at each destabilizing velocity and poor at each restabilizing velocity. There is a mistake somewhere in the original results. The information just presented, coupled with the good-to-excellent agreement between the original and recomputed results in Graph III-B, and the large percentage differences between the original and recomputed flutter velocities shown in Table 3 for figures 6(c) and 6(d), strongly suggests that the mistake is in the original results in figure 6.

Graph III-C. – Graph III-C shows the effect of increasing values of x_β, the distance from the aileron hinge to the aileron center of gravity, on the normalized flutter velocity, $\frac{v_f}{b\omega_\alpha}$, with $\left(\frac{\omega_\beta}{\omega_\alpha}\right)^2$ as the parameter.

Graph III-C uses the following physical constants as –

– discrete values: $a = -0.4$; $b = 6$; $c = 0.5$; $\kappa = \frac{1}{10}$; $r_\alpha^2 = \frac{1}{4}$; $r_\beta^2 = \frac{1}{160}$; $\omega_\alpha = 90$; $g_\alpha = 0$; $g_\beta = 0$; $\xi = 1$.

In terms of their respective axes and parameters, this graph is analogous to Graphs II-B and II-E for Case 2. The shapes of the curves and symbols in this graph are similar to those in the left-most portions of graphs II-B and II-E, all indicating hump modes.

In Graph III-C, except for the blue curve and symbols, the agreement between the original and recomputed results ranges from good to excellent. The blue curve and symbols represents the condition of identical torsion and aileron natural frequencies. For this condition, the original results predict no flutter below a value of x_β of 0.01, while the recomputed results predict flutter at less than half this value.

Observations. – The graphs for Case 3 contain three parametric variations. The original and recomputed results are all hump modes and always show the same trends with increases or decreases in the value of the parameter. With some exceptions (for $x_\beta = 0.0020$ in Graph III-B and for $\left(\frac{\omega_\beta}{\omega_\alpha}\right)^2 = 1$ in Graph III-C), the magnitudes of the original and recomputed results agree with each other very well.

IX. RECURRING DIFFERENCE BETWEEN *NACA 685* RESULTS AND RECOMPUTED RESULTS

A recurring difference was observed between the *NACA 685* results and the present recomputed results. This difference can be found in figure 26; Graph I-A parts (e), (f), (h), (i), (k) through (q); Graph I-D part (b); and Graph I-G. Hints of this recurring difference can be found in parts of Graphs II and III. All of these examples are plots of flutter velocity, v_f, or normalized flutter velocity ($\frac{v_f}{b\omega}$ for this discussion) as a function of the appropriate ratio of natural frequencies ($\frac{\omega}{\omega}$ for this discussion). The difference was observed in both single flutter modes and hump modes. When occurring in hump modes, it manifests in the destabilizing-velocity portion of the curve.

In each instance of this recurring difference, the original curve starts at $\frac{\omega}{\omega} = 0$ with a very shallow negative slope. With increasing $\frac{\omega}{\omega}$, the original curve describes an "elongated-backwards-S" shape: an initial gradual decrease in v_f or $\frac{v_f}{b\omega}$ followed by a more rapid decrease, reaching a minimum and then increasing again. Near the minimum the original curve may be approximated very well by the arc of a circle whose diameter is a significant fraction of the length of the horizontal axis. The blue curves in parts (h) and (l) of Graph I-A are excellent examples of this shape.

In each instance of this recurring difference, the recomputed curve initially follows very closely the original curve. But, with increasing $\frac{\omega}{\omega}$, as the minimum of the original curve is approached, the recomputed curve departs from the original curve. Here the recomputed curve is characterized by steeper, nearly linear slopes, both before and after the original minimum, reaching its own minimum by forming an approximate "V" feature. The bottom of the V frequently has a lower value of v_f or $\frac{v_f}{b\omega}$ than the original minimum has.

It is speculated that this recurring difference is due to the original results being computed at fewer values of $\frac{\omega}{\omega}$ than were the recomputed results, causing the original results to skip over and miss the V feature.

X. CONCLUDING REMARKS

In the year 2000 in an Engineering Note, Zeiler made generally known that three foundational NACA reports and two early aeroelasticity texts contained numerical errors in some of their numerical examples. Zeiler recommended that an effort be undertaken to employ the computational resources available today (digital computers) to recompute the numerical examples in these early works and to publish the results so as to provide a complete and error-free set of numerical examples. A multiyear effort is underway that follows Zeiler's recommendation by recomputing the numerical examples in these three NACA reports. The present paper summarizes the recomputations for the second of these reports, *NACA 685*.

The recomputations were performed in Matlab® employing the solution method of *NACA 685*. Comparisons between the original and recomputed results were accomplished by superimposing the latter on the former in the *NACA 685* original figures and graphs. The figures contain comparisons of the raw form of the *NACA 685* solution method for two- and three-degrees-of-freedom (2DOF and 3DOF) flutter problems as well as comparisons of multiple flutter solutions for 2DOF flutter problems. The graphs contain comparisons for many parametric variations for all three cases of the 2DOF flutter problem. The important conclusions regarding the comparisons are:

Raw form results (figs. 1 through 7) –

(1) The shapes of the original and recomputed real loci agree with each other very well for all three 2DOF flutter problems and the 3DOF flutter problem;
(2) The shapes of the original and recomputed imaginary loci agree with each other very well for two of the three 2DOF flutter problems and the 3DOF flutter problem;
(3) For results that contain proper intersections (instances of predicted flutter), there is an approximate inverse relationship between the original value of $1/k$ at the proper intersection and the corresponding percentage difference between the original and recomputed values of $1/k$ at the proper intersection – when one is low the other is high, and vice versa.

Parameter variations (figs. 8, 17, 18, and 26 and graphs) –

(1) The magnitudes of the original and recomputed results ranged from excellent to poor;
(2) With some notable exceptions, the shapes of the original and recomputed curves generally agreed;
(3) The original and recomputed results always show the same trends with increases or decreases in the value(s) of the parameter(s);
(4) For the figures and graphs whose abscissas are the ratio of natural frequencies –
    (a) the agreement between the original and recomputed results is generally better at the lower values of the ratio of natural frequencies than it is at the higher values;
    (b) a recurring difference between original and recomputed results was observed characterized by an “elongated-backwards-S” shape for the original results and by a steep “V” feature for the recomputed results.

Self-consistency of results within *NACA 685* –

Because of the many parameter variations presented in *NACA 685*, there are a few instances of repetition – a flutter result computed using a certain combination of physical constants that appears in one figure or graph also appears in another – providing opportunities to check self-consistency of results within *NACA 685*. Self-consistency of results within *NACA 685* were mixed. Flutter velocities that should have been identical from one figure or graph to another figure or graph exhibited differences from near zero to over 50 percent.

There were two opportunities to check the present recomputations, both of them successful:

(1) Roughly one out of every three or four of the present recomputations were spot checked using the p-method of flutter solution (also performed in Matlab®) with excellent agreement between recomputations and spot-checks –

– In almost all instances agreeing within 0.5 percent of each other, with no difference exceeding two percent.

– Single flutter modes predicted by the method of *NACA 685* were confirmed as single flutter modes by the p-method; hump modes were confirmed as hump modes.

(2) Zeiler's engineering note contained figures illustrating differences he found between his recomputations and Theodorsen's and Garrick's original results. Two of Zeiler's figures corresponded to results in the present paper. Comparisons of Zeiler's recomputations and present recomputations revealed that, in almost all cases, Zeiler's and present recomputations were either coincident or nearly coincident with each other.

These opportunities provided confidence that the recomputed results were correct, especially for those instances when the original results and recomputed results differed significantly.

Given that the original results were obtained "by hand" with pencils, paper, slide rules, and comptometers, with some notable exceptions, the agreement between the original and recomputed results (in terms of magnitudes, shapes of curves, trends with variations in parameters) was surprisingly good.

APPENDIX A

BRIEF DESCRIPTIONS OF THEODORSEN'S AND GARRICK'S TRILOGY OF PAPERS ON FLUTTER

This appendix presents brief descriptions of Theodorsen's and Garrick's trilogy of papers on flutter:

NACA 496 Theodorsen, Theodore: *General Theory of Aerodynamic Instability and the Mechanism of Flutter*. NACA Report No. 496, from 20th Annual Report of the National Advisory Committee for Aeronautics, 1934, pp. 413-433.

NACA 685 Theodorsen, Theodore; and Garrick, I. E.: *Mechanism of Flutter, a Theoretical and Experimental Investigation of the Flutter Problem*. NACA Report No. 685, from 26th Annual Report of the National Advisory Committee for Aeronautics, 1940, pp. 101-146.

NACA 741 Theodorsen, Theodore; and Garrick, I. E.: *Flutter Calculations in Three Degrees of Freedom*. NACA Report No. 741, from 28th Annual Report of the National Advisory Committee for Aeronautics, 1942, pp. 223-240.

All three papers address the aeroelastic flutter of a typical section with degrees of freedom: torsion (α), aileron deflection (β), and vertical deflection (h). The equations of motion (shown in equations (A), (B), and (C) in the main body of the present paper) are used in all three papers. These equations are comprised of structural and aerodynamic terms and are written as three simultaneous second-order differential equations in the three unknowns α, β, and h. Equation (A) defines the sum of the moments about the elastic axis; equation (B), the sum of the moments about the aileron hinge; and equation (C), the sum of the forces on the entire "wing" in the vertical direction. Unsteady circulatory aerodynamics are present in the equations in the form of Theodorsen's circulation function, $C(k)$.

In all three papers, the form of the unknowns is chosen to be sinusoidal

$$x = x_0 e^{i(k\frac{v}{b}t+\theta)}$$

where x_0 is the infinitesimal amplitude of unknown x (representing α, β, or h) and θ is the phase angle of x with respect to some reference. When these forms and their time derivatives are substituted into the differential equations, the equations are transformed into three simultaneous algebraic equations with complex coefficients.

By sequentially eliminating one of the equations and its corresponding degree of freedom, the three-degrees-of-freedom (3DOF) flutter equations reduce to three unique cases of two-degrees-of-freedom (2DOF) flutter equations: (h and α), (h and β), and (α and β). These equations are normalized, producing within them products $\Omega_\alpha X$, $\Omega_\beta X$, and $\Omega_h X$, which are central to the solution of these equations.

Within the trilogy, the manner of solving the flutter equations differs from paper to paper, ultimately producing three different solution methods. But, the following solution elements are common to the three papers:

1. Expanding the determinant of the equations, resulting in either a cubic equation in X with complex coefficients (for the 3DOF flutter problem) or a quadratic equation in X with complex coefficients (2DOF), both with right hand sides equal to zero;
2. Separating the real and imaginary parts of the cubic or quadratic equation, with the right hand side of each part equal to zero;
3. Temporarily treating quantity X (and, in one paper, another quantity as well) as a parameter and later treating it (and the other) as a known quantity;
4. Solving the real and imaginary equations at many values of the inverse of reduced frequency, $1/k$;
5. Creating plots from these many solutions, enabling the graphical determination of the flutter velocity, v_f, and flutter reduced frequency, k_f.

All three solution methods are capable of predicting single flutter modes and hump modes. All three papers provide numerical examples. *NACA 496* and *NACA 685* include among their examples plots illustrating their respective raw form solutions (corresponding to solution element 5, above).

NACA 496

NACA 496 presents and employs one method specifically for the solution of the 2DOF flutter problem (referred to in this appendix as Solution Method 1) and outlines, but does not employ, a second method for the solution of the 3DOF flutter problem (Solution Method 2, which may also be used to solve the 2DOF flutter problem). *NACA 496* presents 13 figures that illustrate Solution Method 1.

The details of Solution Method 1 are contained in reference 7, but a brief outline is offered here. As mentioned in the main body of the present paper, Solution Method 1 is complicated.

For this outline of Solution Method 1, the 2DOF flutter equations with α and β as unknowns are chosen as representative of the three sets of the 2DOF flutter equations. In the main body of the present paper, equations (4), (5a), and (5b), and (with modifications) equations (7a) and (7b) are the applicable equations. Because *NACA 496* did not include structural damping in its formulation, imagine equations (7a) and (7b) with structural damping terms g_α and g_β set to zero. Because *NACA 496* did not include a modal coupling factor, imagine equation (7a) with ξ set to unity.

Through judicious choices of quantities ω_r and r_r, Solution Method 1 sets quantity Ω_β to unity, thereby effectively eliminating it from the problem. This step leaves in the problem Ω_α as the only square of a nondimensional frequency ratio. Quantities X and Ω_α are treated as parameters, not as the known quantities expressed in equations (4) and (5a). The real and imaginary equations are solved for X and Ω_α conventionally by substitution at many values of the inverse of reduced frequency. A new quantity, F, is introduced that is proportional to the inverse square root of X. From the many solutions, two curves are produced, Ω_α vs. $1/k$ and F vs. Ω_α, that represent a family of flutter solutions; each point on the first curve has a corresponding point on the second and each pair of corresponding points represents a unique flutter solution. The notion that X and Ω_α are parameters is abandoned and a

problem-specific value of Ω_α is chosen. Flutter reduced frequency is determined from the plot of Ω_α vs. $1/k$; flutter velocity is determined from the plot of F vs. Ω_α.

NACA 685

NACA 685 employs Solution Method 2 to solve both 2DOF and 3DOF flutter problems. *NACA 685* presents 11 figures and three graphs (each containing parameter variations) that illustrate Solution Method 2.

The details of Solution Method 2 are contained in section III of the present paper, but for the sake of the completeness of this appendix, a brief outline is offered here. As the authors of *NACA 685* state, Solution Method 2 is "simpler" than Solution Method 1.

For this outline of Solution Method 2, the 2DOF flutter equations with α and β as unknowns are again chosen as representative of the three sets of the 2DOF flutter equations. Again, equations (4), (5a), (5b), (7a) and (7b) are the applicable equations. Solution Method 2 allows structural damping terms g_α and g_β and modal coupling factor, ξ.

In Solution Method, 2 quantity X is treated as a parameter, while Ω_α and Ω_β are treated as constants. The real and imaginary equations are solved for X for many values of the inverse of the reduced frequency. For the 2DOF flutter problem with nonzero values of g_α and g_β, the real and imaginary equations are both quadratic in X. Thus, each equation produces two roots at each value of $1/k$. Because, from equation (4), X is proportional to the square of velocity, only the nonnegative values of X have physical meaning. The square roots of the nonnegative roots from the real and imaginary equations are plotted as functions of $1/k$ on the same set of axes, forming "real" loci and "imaginary" loci. Intersections of any real locus with any imaginary locus are simultaneous solutions of the real and imaginary equations and define a flutter condition. At these intersections, flutter reduced frequency is determined from the value of the abscissa and flutter velocity is determined from the value of the ordinate.

NACA 741

NACA 741 employs Solution Method 3 to solve only 3DOF flutter problems. *NACA 741* presents 40 figures (each containing a parameter variation) that illustrate Solution Method 3.

Solution Method 3 is similar to Solution Method 2 in that it allows structural damping terms g_α and g_β and modal coupling factor, ξ, and it produces real and imaginary loci. But, in Solution Method 3 there is only a single real locus and a single imaginary locus. These single loci are the result of transforming the real and imaginary equations from their original orders in X to linear equations in X. The transformation is accomplished via a method analogous to Sylvester's method of elimination (ref. 11).

Again, only the nonnegative values of X have physical meaning. As with Solution Method 2, the square roots of the nonnegative roots from the real and imaginary equations are plotted as functions of $1/k$ on the same set of axes and intersections of the real locus with the imaginary locus are simultaneous solutions of the real and imaginary equations and define a flutter condition. As with Solution Method 2, at these intersections, flutter reduced frequency is determined from the value of the abscissa and flutter velocity is determined from the value of the ordinate.

APPENDIX B

COMPARISON OF ZEILER'S RECOMPUTATIONS WITH PRESENT RECOMPUTATIONS

In his Engineering Note (EN) appearing in the September-October 2000 issue of the Journal of Aircraft (ref. 1), Zeiler made generally known that errors existed in some of the plots in Theodorsen's and Garrick's (T&G's) trilogy of papers on flutter. Zeiler did this by electronically scanning T&G's results and then superimposing his own results, thereby providing clear comparisons. As Zeiler states in his EN, his recomputations were performed in Matlab® employing the standard V-g method of flutter analysis.

Zeiler's EN contained three comparison figures, two of which (Zeiler's figs. 2 and 3) featured T&G's flutter results that originally appeared in *NACA 685*, and were later reproduced in references 5 and 6. (T&G's flutter results in Zeiler's third comparison figure appeared originally in *NACA 741.*) For his figures 2 and 3, Zeiler chose to scan the versions of T&G's original results that appear in reference 6.

The following table shows the progression of these particular sets of T&G's flutter results through the various sources:

Corresponding Figure and Graph Numbers in -		
NACA 685 (ref. 3)	Bisplinghoff & Ashley (ref. 6)	Zeiler (ref. 1)
Graph I-A, part (q)	Figure 6-18	Figure 2
Graph I-C, part (h)	Figure 6-19	Figure 3

From this table, it is seen that Zeiler's original figures 2 and 3 derive from Graphs I-A and I-C, which are 2DOF numerical examples for Case 1. Zeiler's figure 2 contains plots of normalized flutter velocity, $\frac{U_f}{b\omega_\alpha}$ ($\frac{v_f}{b\omega_\alpha}$ in the notation of the present paper), as a function of frequency ratio $\frac{\omega_h}{\omega_\alpha}$. Zeiler's figure 3 contains plots of normalized flutter velocity as a function of mass ratio, μ ($1/\kappa$ in the notation of the present paper); the abscissa in Zeiler's figure 3 extends to $\mu = 100$, while that in part (h) of Graph I-C extends only to $1/\kappa = 30$.

Fortuitously and importantly, Zeiler's figures 2 and 3 provide an opportunity to compare Zeiler's recomputations with present recomputations. Figures B1 and B2 of this appendix correspond, respectively, to Zeiler's figures 2 and 3, with present recomputations superimposed.

Zeiler's figures 2 and 3 are "busy" in the same way that the Graphs in the present paper are busy: each containing multiple original curves representing T&G's results and multiple sets of superimposed symbols representing Zeiler's recomputed results. Comparing Zeiler's recomputations and present recomputations requires the addition of even more sets of superimposed symbols, creating the potential to compound the busy-ness in the figures. To avoid this extra busy-ness and to make the comparisons between Zeiler's recomputations and present recomputations clear and easy to discern,

figures B1 and B2 in this appendix each contain four parts – one part for each value of the parameter x_α. Part (a) of each figure contains Zeiler's entire original figure and present recomputations for only $x_\alpha = 0$; part (b) of each figure contains Zeiler's entire original figure and present recomputations for only $x_\alpha = 0.05$; and so forth. Also in the interest of clarity, in figures B1 and B2, Zeiler's original keys have been removed and are replaced with keys that reflect the addition of the present recomputations: Zeiler's recomputations are depicted by black symbols and present recomputations are depicted by red symbols.

Figure B1

In parts (b), (c), and (d) of figure B1, Zeiler's recomputations and the present recomputations are seen to agree extremely well – coincident or nearly coincident in all cases. This extremely good agreement is also apparent in part (a) of figure B1 for values of $\frac{\omega_h}{\omega_\alpha}$ of 0.5 and higher, but for lower values of $\frac{\omega_h}{\omega_\alpha}$, there are some noticeable differences between Zeiler's and the present recomputations. However, at $\frac{\omega_h}{\omega_\alpha} = 0.3$, this noticeable difference is only on the order of four percent.

Figure B2

In all parts of figure B2, Zeiler's recomputations and the present recomputations are seen to agree extremely well – coincident or nearly coincident in all cases.

Observations

Eight different comparisons (four each in figs. B1 and B2) of Zeiler's recomputations and the present recomputations of T&G's normalized flutter velocities agree with each other very well. Not available were comparisons of the corresponding flutter reduced frequencies. The consistently good agreement between Zeiler's and the present recomputations gives additional confidence that the present recomputations are correct.

REFERENCES

1. Zeiler, Thomas A.: *Results of Theodorsen and Garrick Revisited*. Journal of Aircraft, Vol. 37, No. 5, Sept-Oct 2000, pp. 918-920.

2. Theodorsen, Theodore: *General Theory of Aerodynamic Instability and the Mechanism of Flutter*. NACA Report No. 496, from 20th Annual Report of the National Advisory Committee for Aeronautics, 1934, pp. 413-433.

3. Theodorsen, Theodore; and Garrick, I. E.: *Mechanism of Flutter, a Theoretical and Experimental Investigation of the Flutter Problem*. NACA Report No. 685, from 26th Annual Report of the National Advisory Committee for Aeronautics, 1940, pp. 101-146.

4. Theodorsen, Theodore; and Garrick, I. E.: *Flutter Calculations in Three Degrees of Freedom*. NACA Report No. 741, from 28th Annual Report of the National Advisory Committee for Aeronautics, 1942, pp. 223-240.

5. Bisplinghoff, R. L.; Ashley, H.; and Halfman, R. L.: *Aeroelasticity*, Addison-Wesley-Longman, Reading, MA, 1955.

6. Bisplinghoff, R. L.; and Ashley, H.: *Principles of Aeroelasticity*, Dover, New York, 1962.

7. Perry, Boyd III: *Re-Computation of Numerical Results Contained in NACA Report No. 496*. NASA TP-2015-218765, June 2015.

8. Richardson, J. R.: *A More Realistic Method for Routine Flutter Calculations.* AIAA Symposium on Structural Dynamics and Aeroelasticity, Boston, MA, Aug. 30 – Sept. 1, 1965, pp. 10-17.

9. Abel, Irving: *An Analytical Technique for Predicting the Characteristics of a Flexible Wing Equipped with an Active Flutter-Suppression System and Comparison with Wind-Tunnel Data*. NASA TP-1367, February 1979.

10. Brunton, Steven L.; and Rowley, Clarence W.: *Empirical State-Space Representations for Theodorsen's Lift Model*. Journal of Fluids and Structures, Vol. 38, April 2013, pp. 174-186.

11. Dickson, Leonard Eugene: *First Course in the Theory of Equations*. John Wiley & Sons, Inc., 1922. (Reprinted by Petra Books, www.petrabooks.com)

Table 1. – Criteria for Qualitative Assessment of Agreement Between Original and Recomputed Results

Qualitative Assessment of Agreement	Criteria for Qualitative Assessment		
	Agreement in magnitudes at a given value of the independent variable		Agreement in overall trends
Excellent	Curve passes through symbol	*and*	Major features of the original curve (max value, min value, slope, inflections) agree with major features of the recomputed results
Good	Curve is within one symbol diameter of symbol	*and*	
Fair	Curve is within three symbol diameters of symbol	*and*	
Poor	Curve is greater than three symbol diameters away from symbol	*or*	Major features of the original curve disagree with major features of the recomputed results

Table 2. – Physical Constants by Figure Number and Case

Figure	*Case*	a	b	c	κ	x_α	r_α^2	x_β	r_β^2	ω_α	ω_β	ω_h	g_α	g_β	g_h	ξ	
1	1	-0.4	6		0.25	0.2	0.25			90		22.5	0		0	1	
2	2		6	0.6	0.25			0	0.0012		27.557	22.5		0	0	1	
3	3	-0.4	6	0.6	0.25		0.25	0	0.0012	90	27.557		0	0		1	
4	3DOF	-0.4	6	0.6	0.25	0.2	0.25	0	0.0012	90	27.557	22.5	0	0	0		
5a	2		6	0.6	0.25			0	0.0012		0	22.5		0	0	1	
5b	2		6	0.6	0.25			0	0.0012		27.557	22.5		0	0	1	*(identical to fig. 2)*
5c	2		6	0.6	0.25			0.0066	0.0012		0	22.5		0	0	1	
5d	2		6	0.6	0.25			0.0066	0.0012		27.557	22.5		0	0	1	
6a	3	-0.4	6	0.6	0.25		0.25	0	0.0012	90	0		0	0		1	
6b	3	-0.4	6	0.6	0.25		0.25	0	0.0012	90	27.557		0	0		1	*(identical to fig. 3)*
6c	3	-0.4	6	0.6	0.25		0.25	0.0066	0.0012	90	0		0	0		1	
6d	3	-0.4	6	0.6	0.25		0.25	0.0066	0.0012	90	27.557		0	0		1	
7a	3DOF	-0.4	6	0.6	0.25	0.2	0.25	0	0.0012	90	0	22.5	0	0	0		
7b	3DOF	-0.4	6	0.6	0.25	0.2	0.25	0	0.0012	90	27.557	22.5	0	0	0		*(identical to fig. 4)*
7c	3DOF	-0.4	6	0.6	0.25	0.2	0.25	0.0066	0.0012	90	0	22.5	0	0	0		
7d	3DOF	-0.4	6	0.6	0.25	0.2	0.25	0.0066	0.0012	90	27.557	22.5	0	0	0		
8	3DOF	-0.4	6	0.6	0.25	0.2	0.25	0	0.0012	90	variable	22.5	0	0	0		
17	1	-0.4	0.5		1/90	0.25	0.3125			113.8		variable	0		0	1	
19	1	-0.4	0.5		1/90	0.25	0.3125			113.8		variable	0		0	1	
26-1	2		0.667	0.5	1/105			0.0076	0.0019		variable	67.104		0	0	1	
26-2	2		0.667	0.5	1/105			0.0076	0.0019		variable	67.104		0	0.0125	1	

Table 3. – Comparison of Original and Recomputed Flutter Results Obtained from Proper Intersections in Figures 1, 4, 5, 6, and 7

Figure	Type Flutter Mode	Calculation	Proper Intersection		Flutter Condition	
			$1/k$	$\sqrt{X}$	v_f , fps	k_f
1	Single	Original [a]	2.460	1.594	833.4	0.407
		Recomputed	2.460	1.592	834.4	0.407
		% Difference	0.0	0.1	0.1	0.0
4	Single	Original [a]	0.875	1.060	445.8	1.143
		Recomputed	0.736	1.064	373.5	1.359
		% Difference	17.3	0.4	17.6	17.3
5(c)	Hump (Destabilizing)	Original [b]	0.250	2.156	31.3	4.000
		Recomputed	0.034	2.156	4.2	29.499
		% Difference	152.2	0.0	152.2	152.2
5(c)	Hump (Restabilizing)	Original [b]	0.713	2.073	92.9	1.402
		Recomputed	0.696	2.072	90.7	1.436
		% Difference	2.4	0.0	2.3	2.4
6(c)	Hump (Destabilizing)	Original [b]	0.220	0.951	124.8	4.550
		Recomputed	0.143	0.969	79.8	6.988
		% Difference	42.3	1.9	44.1	42.3
6(c)	Hump (Restabilizing)	Original [b]	0.857	0.945	489.6	1.167
		Recomputed	1.070	1.036	557.6	0.935
		% Difference	22.1	9.2	13.0	22.1
6(d)	Hump (Destabilizing)	Original [b]	0.258	0.967	144.1	3.874
		Recomputed	0.203	0.963	113.7	4.933
		% Difference	24.0	0.5	23.6	24.0
6(d)	Hump (Restabilizing)	Original [b]	0.807	0.956	455.4	1.240
		Recomputed	1.004	1.021	531.2	0.996
		% Difference	21.8	6.5	15.4	21.8
7(a)	Single	Original [b]	0.780	1.087	387.5	1.283
		Recomputed	0.705	1.061	358.8	1.418
		% Difference	10.1	2.4	7.7	10.1
7(b)	Single	Original [b]	0.852	1.121	410.7	1.173
		Recomputed	0.736	1.064	373.5	1.359
		% Difference	14.6	5.2	9.5	14.6
7(c)	Hump (Destabilizing)	Original [b]	0.153	4.340	19.0	6.557
		Recomputed	0.038	4.331	4.7	26.579
		% Difference	120.8	0.2	120.7	120.8
7(c)	Hump (Restabilizing)	Original [b]	0.678	4.162	88.0	1.475
		Recomputed	0.698	4.154	90.7	1.433
		% Difference	2.9	0.2	3.1	2.9
7(c)	Single	Original [b]	0.171	0.905	102.0	5.851
		Recomputed	0.182	0.885	111.0	5.499
		% Difference	6.2	2.3	8.5	6.2
7(d)	Single	Original [b]	0.187	0.888	113.7	5.345
		Recomputed	0.234	0.884	143.1	4.270
		% Difference	22.4	0.5	22.9	22.4

[a] Values of $1/k$, $\sqrt{X}$, and v_f given in text of *NACA 685*

[b] Values of $1/k$ and $\sqrt{X}$ read from original figure in *NACA 685*

Table 4. – Arrangement of Parts of Graph I-A

$b = 6;\ r_\alpha^2 = 0.25;\ \omega_\alpha = 90;\ \omega_h$ = *variable*

$g_\alpha = 0;\ g_h = 0;\ \xi = 1$

x_α = *parameter*

		Part of graph for values of κ of -					
		1/2	**1/3**	**1/4**	**1/5**	**1/10**	**1/20**
Part of graph for values of a of -	**-0.2**	(c)	(f)	(i)	(l)	(o)	(r)
	-0.3	(b)	(e)	(h)	(k)	(n)	(q)
	-0.4	(a)	(d)	(g)	(j)	(m)	(p)
	-0.45				(s)	(t)	(u)

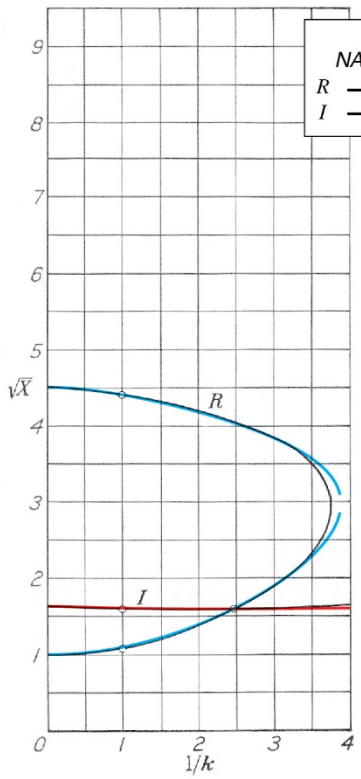

FIGURE 1.—Case 1. Numerical example. The roots $\sqrt{X}$ of the real and the imaginary equations against $1/k$.

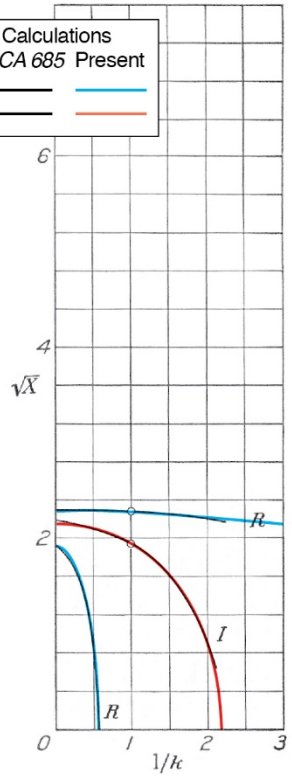

FIGURE 2.—Case 2. Numerical example. The roots $\sqrt{X}$ of the real and the imaginary equations against $1/k$.

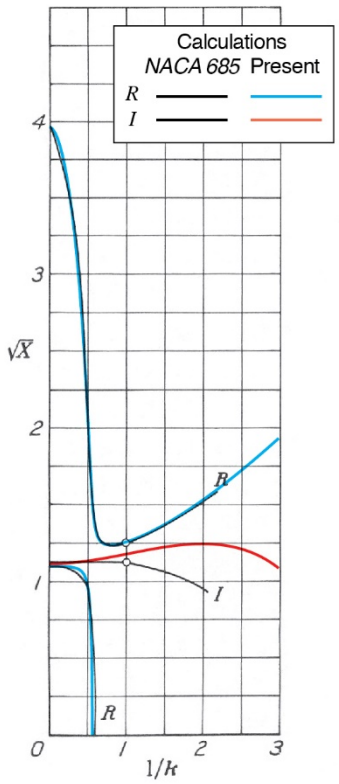

FIGURE 3.—Case 3. Numerical example. The roots $\sqrt{X}$ of the real and the imaginary equations against $1/k$.

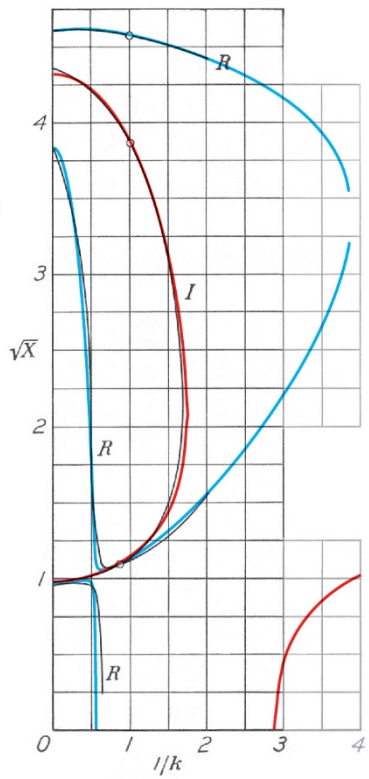

FIGURE 4.—Three degrees of freedom. Numerical example. The roots $\sqrt{X}$ of the real and the imaginary equations against $1/k$.

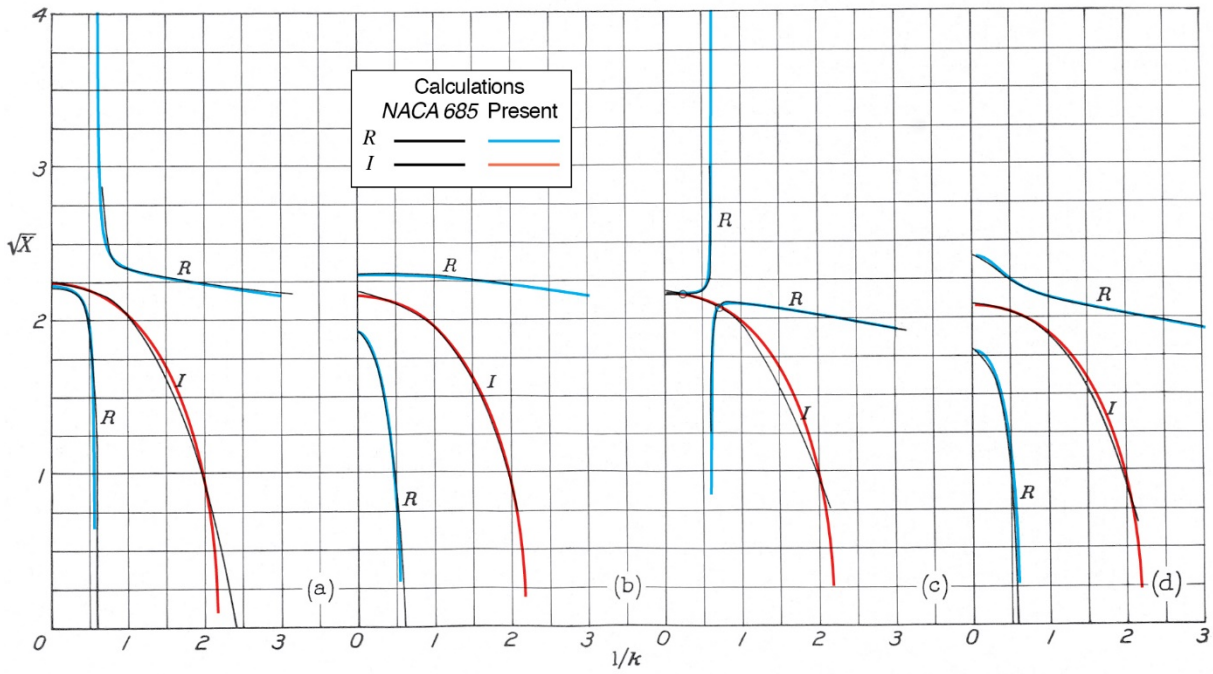

(a) $\left(\frac{\omega_\beta}{\omega_h}\right)^2=0;\ x_\beta=0.$ (b) $\left(\frac{\omega_\beta}{\omega_h}\right)^2=3/2;\ x_\beta=0.$ (c) $\left(\frac{\omega_\beta}{\omega_h}\right)^2=0;\ x_\beta=0.0066.$ (d) $\left(\frac{\omega_\beta}{\omega_h}\right)^2=3/2;\ x_\beta=0.0066.$

FIGURE 5.—Case 2. The roots $\sqrt{X}$ of the real and the imaginary equations against $1/k$. Same parameters as in numerical example except as indicated.

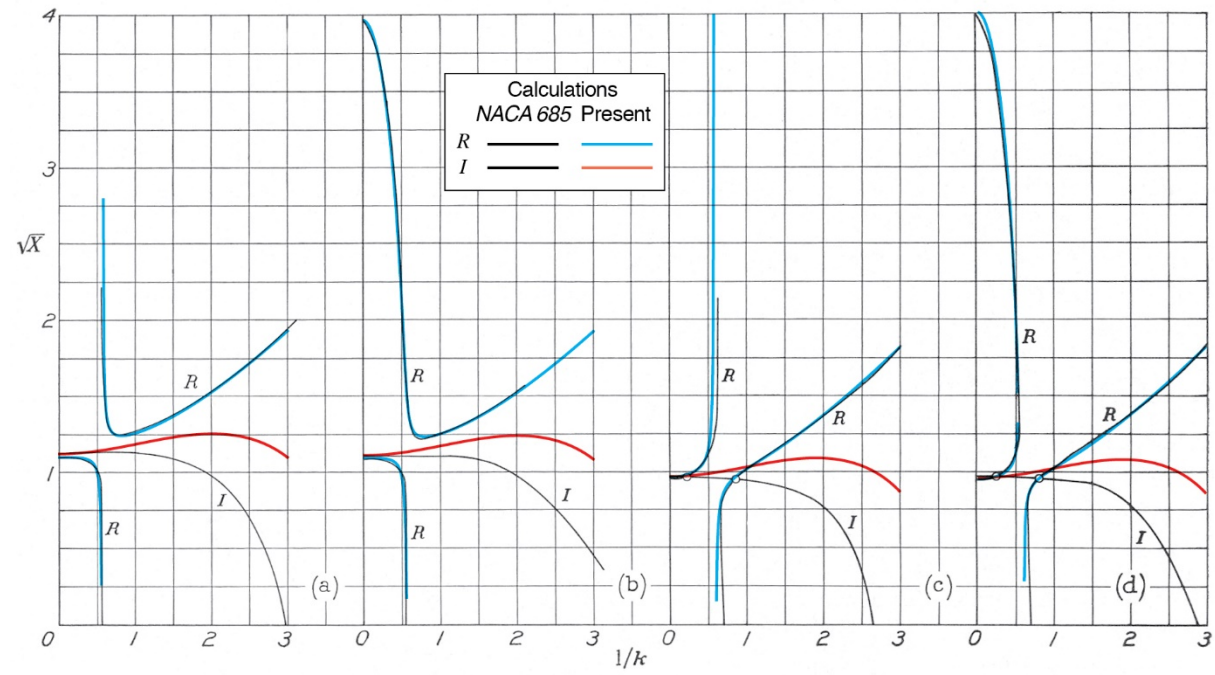

(a) $\left(\frac{\omega_\beta}{\omega_\alpha}\right)^2=0;\ x_\beta=0.$ (b) $\left(\frac{\omega_\beta}{\omega_\alpha}\right)^2=3/32;\ x_\beta=0.$ (c) $\left(\frac{\omega_\beta}{\omega_\alpha}\right)^2=0;\ x_\beta=0.0066.$ (d) $\left(\frac{\omega_\beta}{\omega_\alpha}\right)^2=3/32;\ x_\beta=0.0066.$

FIGURE 6.—Case 3. The roots $\sqrt{X}$ of the real and the imaginary equations against $1/k$. Same parameters in numerical example except as indicated.

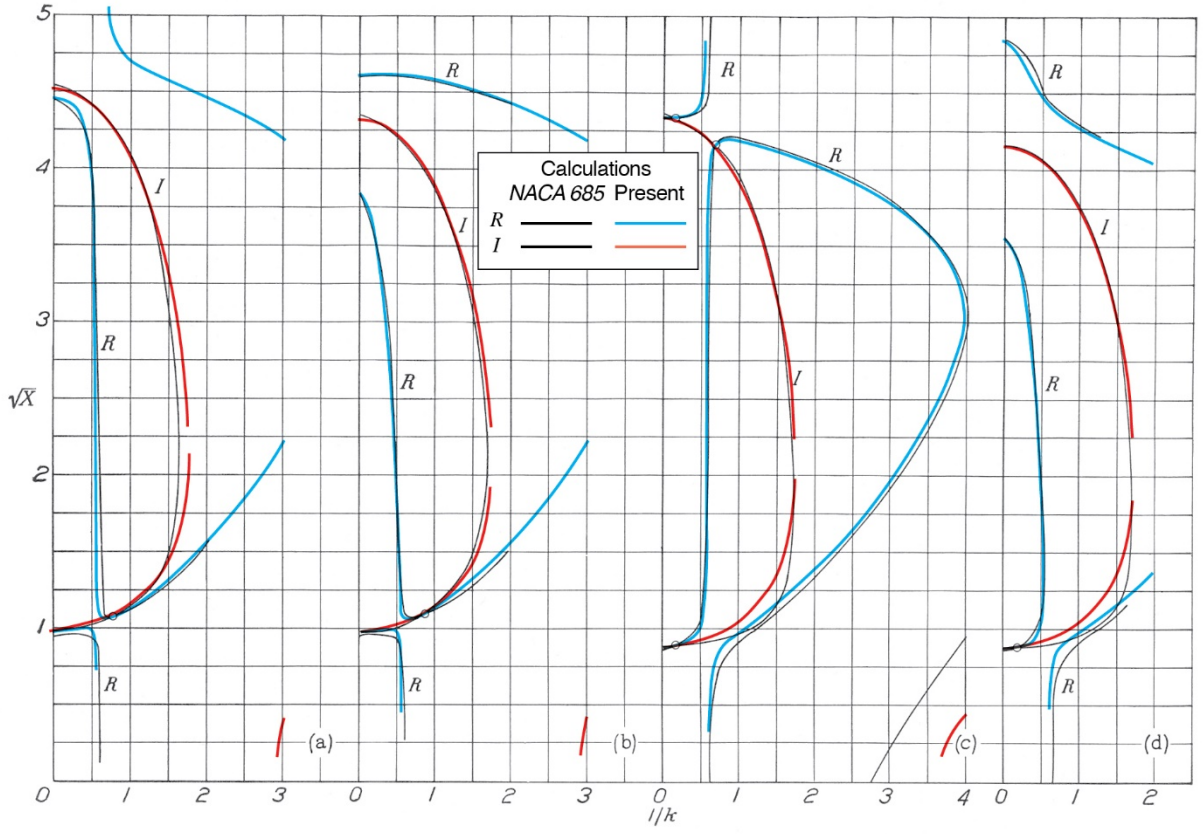

(a) $\left(\frac{\omega_\beta}{\omega_h}\right)^2=0$; $x_\beta=0$. (b) $\left(\frac{\omega_\beta}{\omega_h}\right)^2=3/2$; $x_\beta=0$. (c) $\left(\frac{\omega_\beta}{\omega_h}\right)^2=0$; $x_\beta=0.0066$. (d) $\left(\frac{\omega_\beta}{\omega_h}\right)^2=3/2$; $x_\beta=0.0066$.

FIGURE 7.—Three degrees of freedom. The roots $\sqrt{X}$ of the real and the imaginary equations against $1/k$. Same parameters as in numerical example except as indicated.

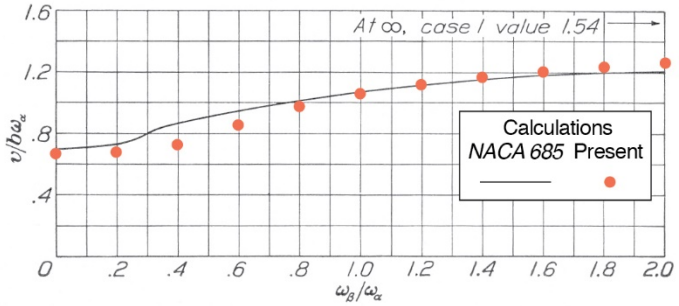

FIGURE 8.—Flutter coefficient against frequency ratio $\omega_\beta/\omega_\alpha$. Three degrees of freedom. $\kappa=0.25$; $a=-0.4$; $x_\alpha=0.2$; $r_\alpha^2=1/4$; $c=0.6$; $x_\beta=0$; $r_\beta^2=0.0012$; $g_\alpha=g_h=0$.

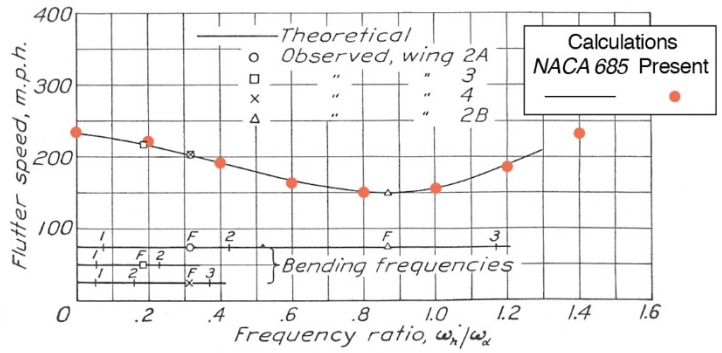

FIGURE 17.—Theoretical flutter speed based on constants pertaining to wings 2A, 2B, 3, and 4. $\kappa=1/90$; $a=-0.4$; $x_\alpha=1/4$; $r_\alpha^2=0.3125$; $b\omega_\alpha=38.8$ miles per hour. Experimental test points are also shown, and flutter modes and frequencies are indicated.

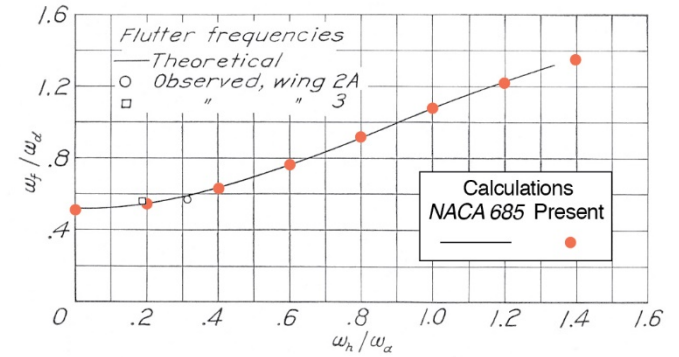

FIGURE 19.—Theoretical flutter frequencies based on constants for wings 2, 3, and 4 with experimentally observed values for wings 2A and 3. $\kappa=1/90$; $a=-0.4$; $x_\alpha=1/4$; $r_\alpha^2=0.3125$. Case 1(h, α).

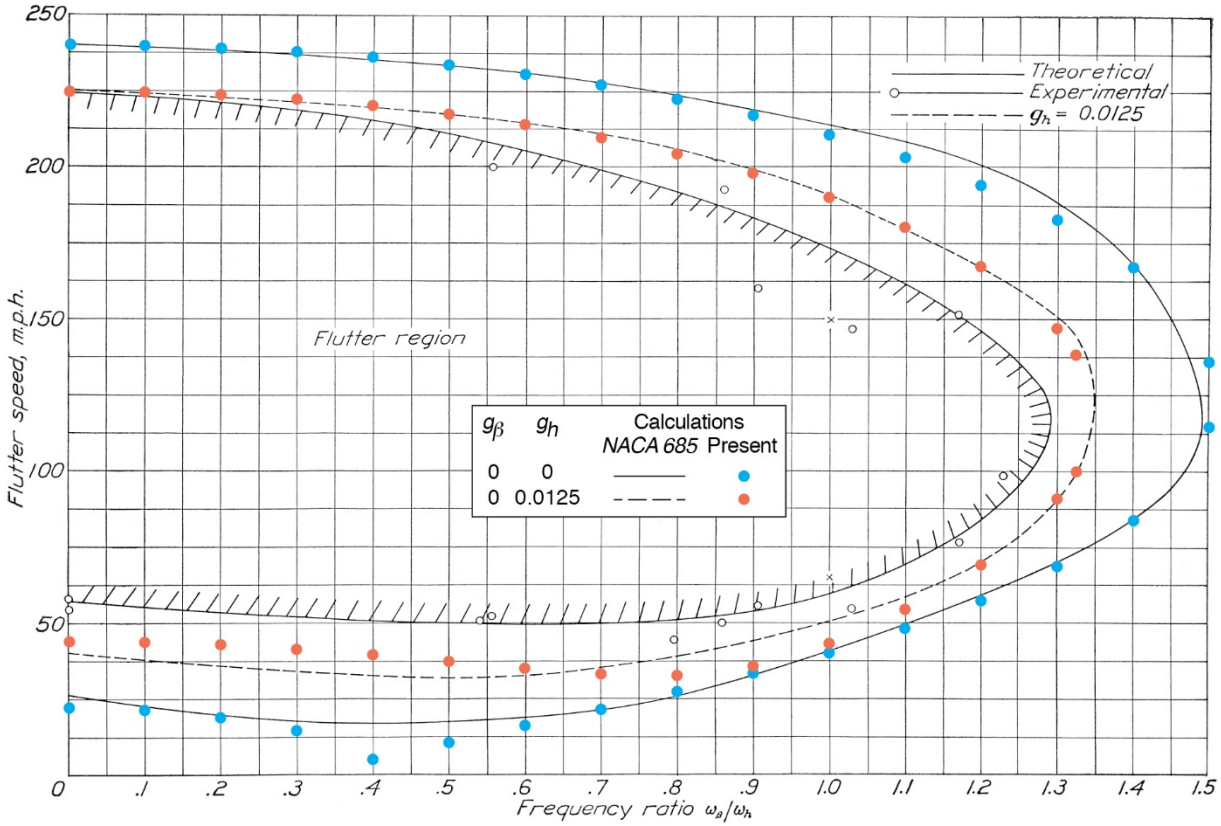

FIGURE 26.—Theoretical flutter speed based on constants pertaining to wing 5 with aileron AII. ($c=\frac{1}{2}$; $x_\beta=0.0076$; $r_\beta^2=0.0019$; $\kappa=\frac{1}{1}\frac{1}{0}\frac{1}{5}$; $b\omega_h=30.5$ m. p. h.) Experimental values are shown; flutter region is shaded. Dashed (theoretical) curve corresponds to friction coefficient $g_h=0.0125$.

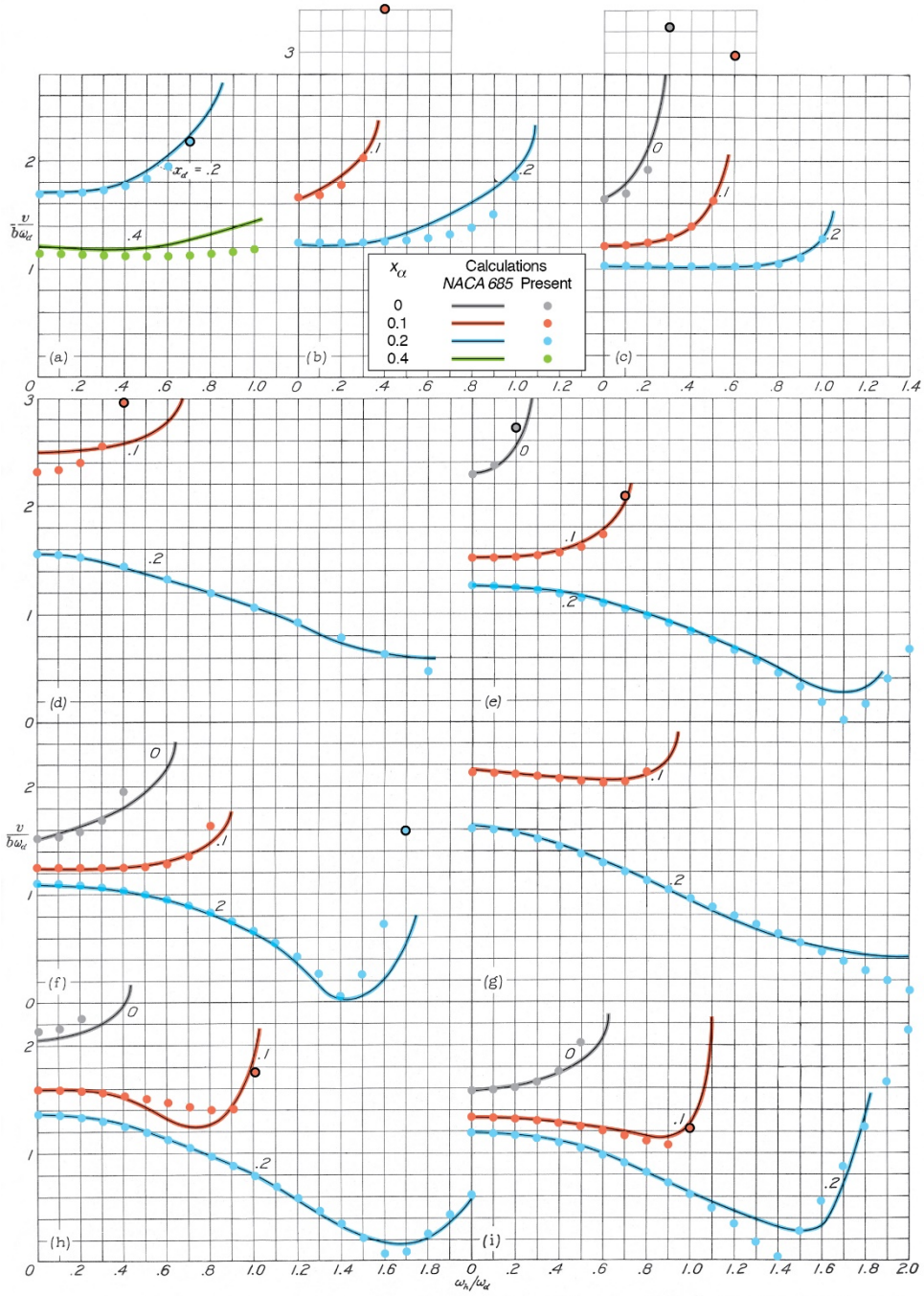

(a) $\kappa=\frac{1}{2}$; $a=-0.4$; $x_\alpha=0$ stable; $x_\alpha=0.1$ stable; $v_D/b\omega_\alpha=1.58$.
(b) $\kappa=\frac{1}{2}$; $a=-0.3$; $x_\alpha=0$ stable; $v_D/b\omega_\alpha=1.12$.
(c) $\kappa=\frac{1}{2}$; $a=-0.2$; $v_D/b\omega_\alpha=0.913$.
(d) $\kappa=\frac{1}{2}$; $a=-0.4$; $x_\alpha=0$ stable; $v_D/b\omega_\alpha=1.94$.
(e) $\kappa=\frac{1}{2}$; $a=-0.3$; $v_D/b\omega_\alpha=1.37$.
(f) $\kappa=\frac{1}{2}$; $a=-0.2$; $v_D/b\omega_\alpha=1.12$.
(g) $\kappa=\frac{1}{4}$; $a=-0.4$; $x_\alpha=0$ stable; $v_D/b\omega_\alpha=2.24$.
(h) $\kappa=\frac{1}{4}$; $a=-0.3$; $v_D/b\omega_\alpha=1.58$.
(i) $\kappa=\frac{1}{4}$; $a=-0.2$; $v_D/b\omega_\alpha=1.29$.

Graph I–A (a–i).—The effect of x_α; the flutter coefficient against the frequency ratio; $r_\alpha^2=1/4$. Case 1 (h, α).

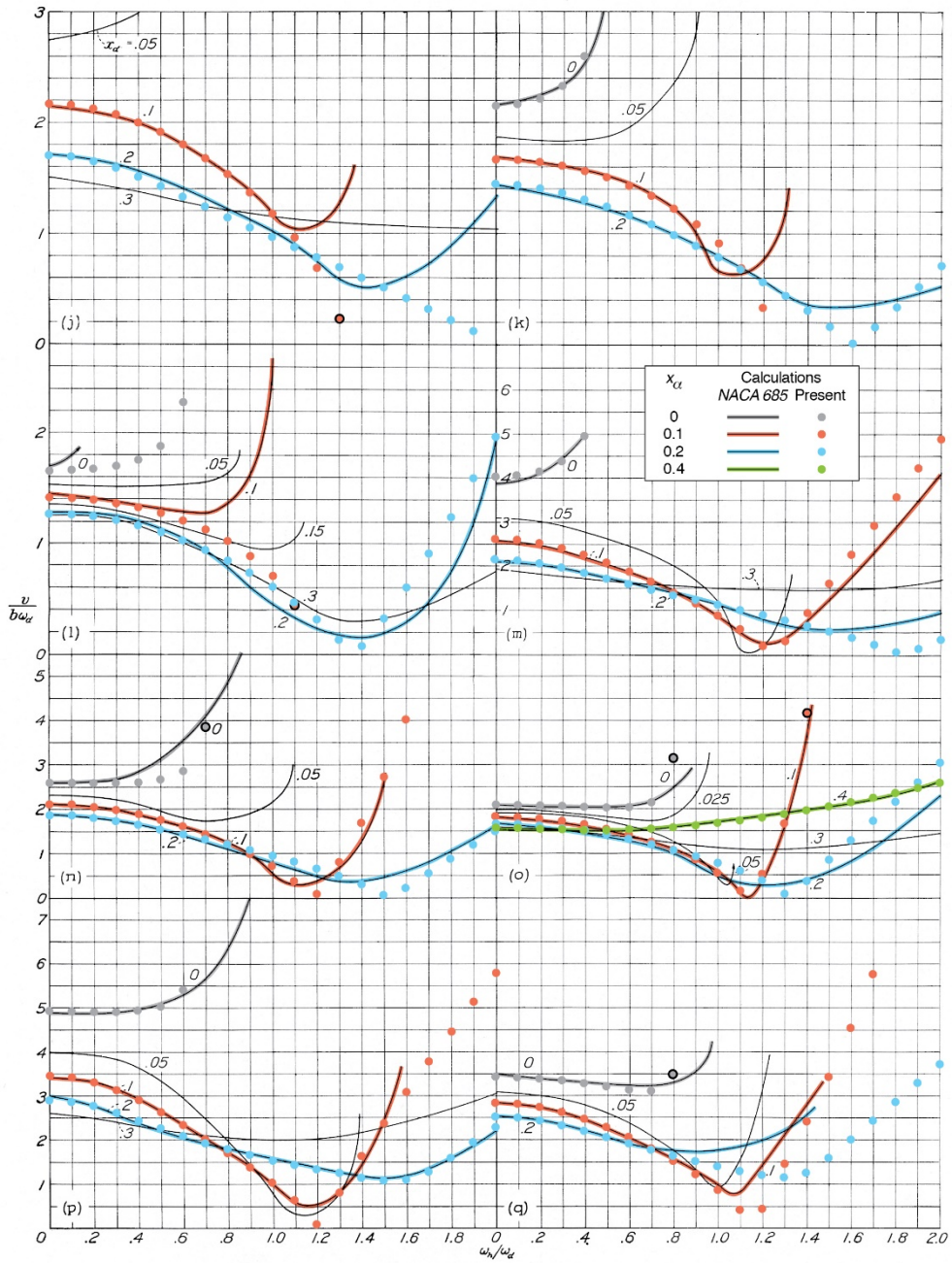

(j) $\kappa=\frac{1}{5}$; $a=-0.4$; $v_D/b\omega_\alpha=2.5$; $x_\alpha=0$, starts at ordinate 6.9.
(k) $\kappa=\frac{1}{5}$; $a=-0.3$; $v_D/b\omega_\alpha=1.77$.
(l) $\kappa=\frac{1}{5}$; $a=-0.2$; $v_D/b\omega_\alpha=1.45$.
(m) $\kappa=\frac{1}{10}$; $a=-0.4$; $v_D/b\omega_\alpha=3.54$.
(n) $\kappa=\frac{1}{10}$; $a=-0.3$; $v_D/b\omega_\alpha=2.5$.
(o) $\kappa=\frac{1}{10}$; $a=-0.2$; $v_D/b\omega_\alpha=2.05$.
(p) $\kappa=\frac{1}{20}$; $a=-0.4$; $v_D/b\omega_\alpha=5.0$.
(q) $\kappa=\frac{1}{20}$; $a=-0.3$; $v_D/b\omega_\alpha=3.54$.

Graph I–A (j–q).—The effect of x_α; the flutter coefficient against the frequency ratio; $r_\alpha^2=1/4$. Case 1 (h, α).

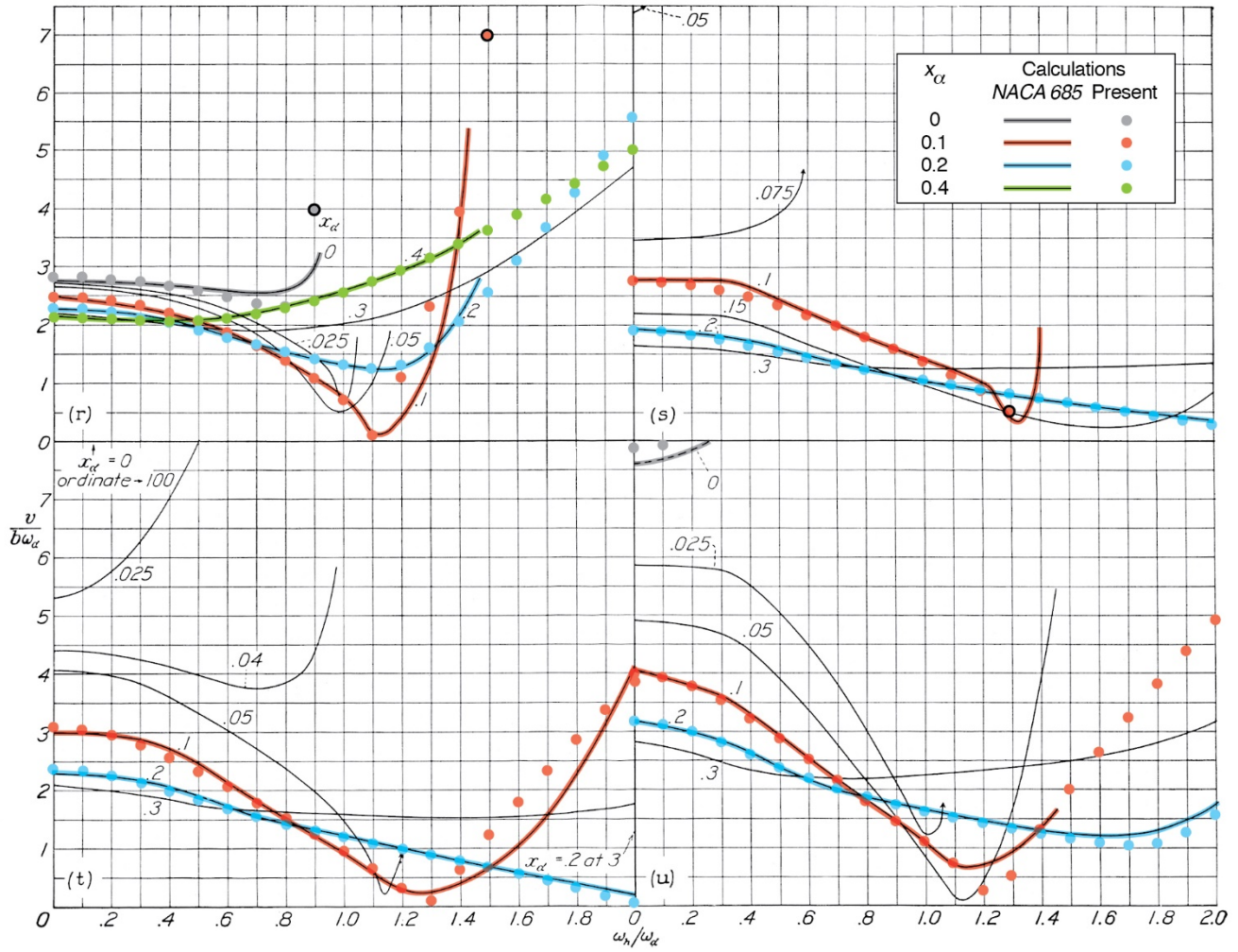

(r) $\kappa=\frac{1}{20}$; $a=-0.2$; $v_D/b\omega_\alpha=2.88$.
(s) $\kappa=\frac{1}{5}$; $a=-0.45$; $v_D/b\omega_\alpha=3.54$.
(t) $\kappa=\frac{1}{10}$; $a=-0.45$; $v_D/b\omega_\alpha=5.0$.
(u) $\kappa=\frac{1}{20}$; $a=-0.45$; $v_D/b\omega_\alpha=7.07$.

Graph I-A (r-u).—The effect of x_α; the flutter coefficient against the frequency ratio; $r_\alpha^2=1/4$. Case 1 (h, α).

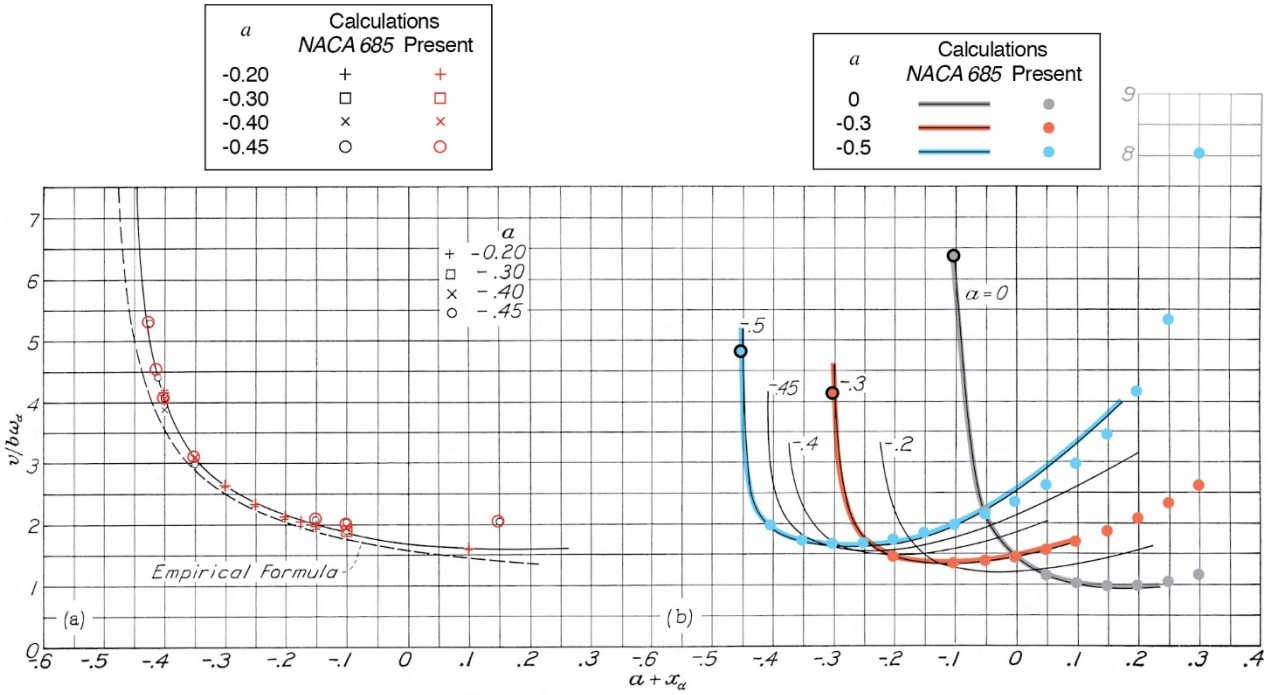

(a) $\kappa=\frac{1}{10}$; $\left(\frac{\omega_h}{\omega_\alpha}\right)^2=0$. (b) $\kappa=\frac{1}{10}$; $\left(\frac{\omega_h}{\omega_\alpha}\right)^2=\frac{1}{2}$.

Graph I–B.—The effect of the stiffness axis; the flutter coefficient against the center-of-gravity location; $r_\alpha^2=1/4$. Case 1 (h, α).

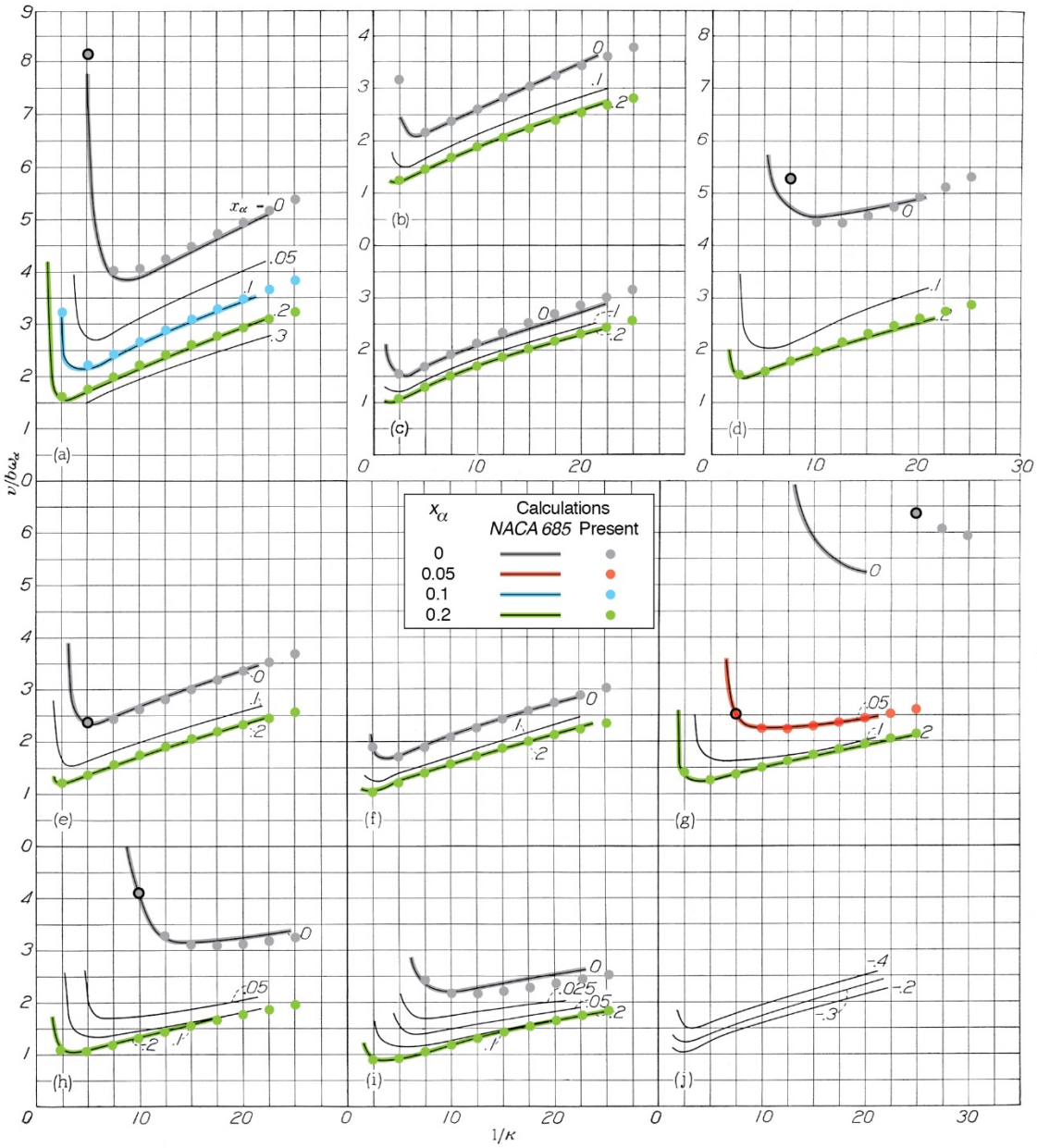

(a) $\left(\frac{\omega_h}{\omega_\alpha}\right)^2=0$; $a=-0.4$.

(b) $\left(\frac{\omega_h}{\omega_\alpha}\right)^2=0$; $a=-0.3$.

(c) $\left(\frac{\omega_h}{\omega_\alpha}\right)^2=0$; $a=-0.2$.

(d) $\left(\frac{\omega_h}{\omega_\alpha}\right)^2=\frac{1}{10}$; $a=-0.4$.

(e) $\left(\frac{\omega_h}{\omega_\alpha}\right)^2=\frac{1}{10}$; $a=-0.3$.

(f) $\left(\frac{\omega_h}{\omega_\alpha}\right)^2=\frac{1}{10}$; $a=-0.2$.

(g) $\left(\frac{\omega_h}{\omega_\alpha}\right)^2=\frac{1}{2}$; $a=-0.4$.

(h) $\left(\frac{\omega_h}{\omega_\alpha}\right)^2=\frac{1}{2}$; $a=-0.3$.

(i) $\left(\frac{\omega_h}{\omega_\alpha}\right)^2=\frac{1}{2}$; $a=-0.2$.

(j) $\left(\frac{\omega_h}{\omega_\alpha}\right)^2=\frac{1}{10}$; $x_\alpha=0.2$. In this section of the graph, the values on the curves refer to a, not to x_α as in sections (a) to (i).

Graph I–C (a–j).—The effect of x_α; the flutter coefficient against $1/\kappa$; $r_\alpha^2=\frac{1}{4}$. Case 1 (h, α).

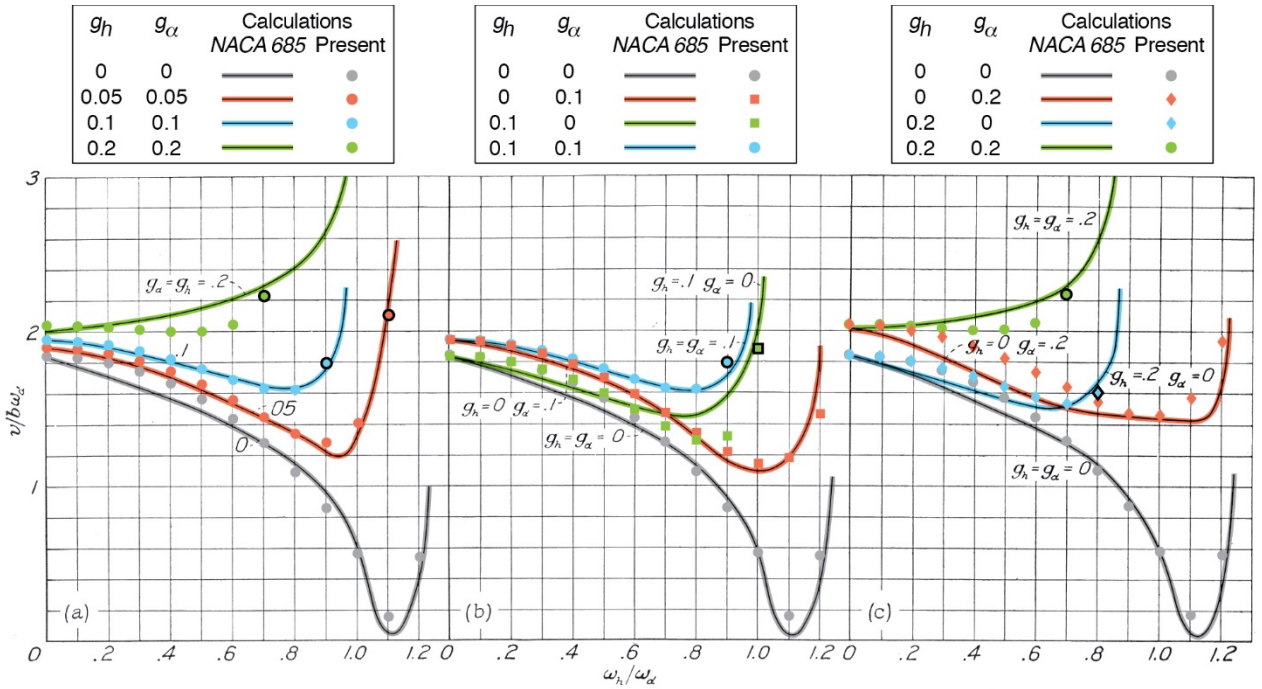

Graph I–D (a–c).—The effect of structural friction; the flutter coefficient against the frequency ratio; $\kappa = 1/10$; $a = -0.2$; $x_\alpha = 0.1$. Case 1 (h, α).

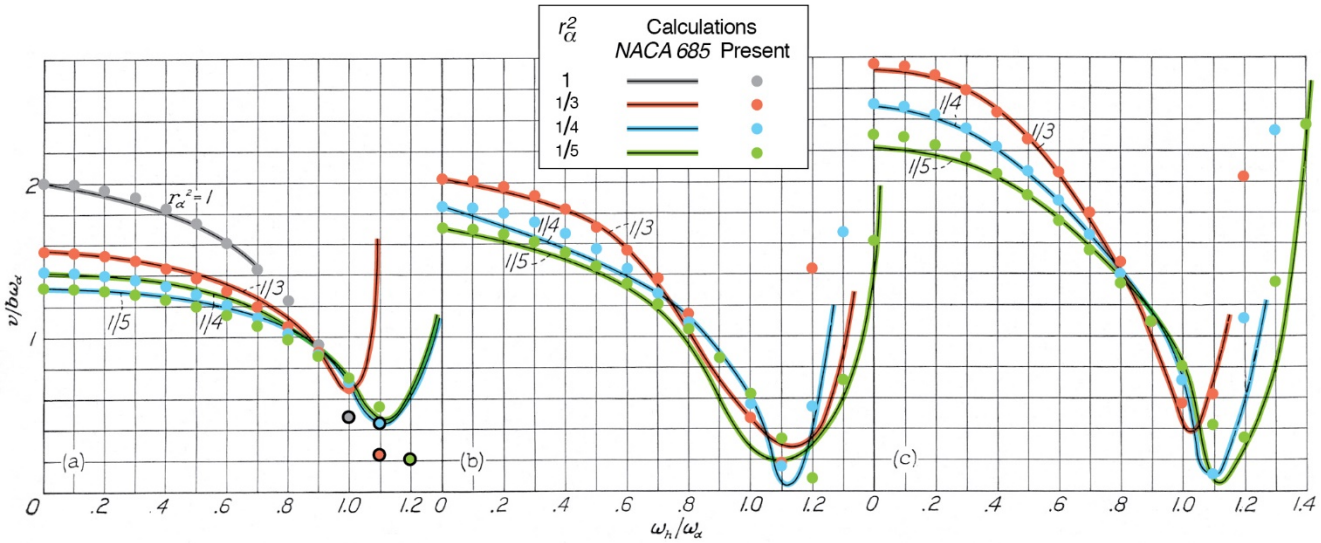

(a) $\kappa = 1/5$. (b) $\kappa = 1/10$. (c) $\kappa = 1/20$.

Graph I–E (a–c).—The effect of radius of gyration; the flutter coefficient against the frequency ratio; $a = -0.2$, $x_\alpha = 0.1$. Case 1 (h, α).

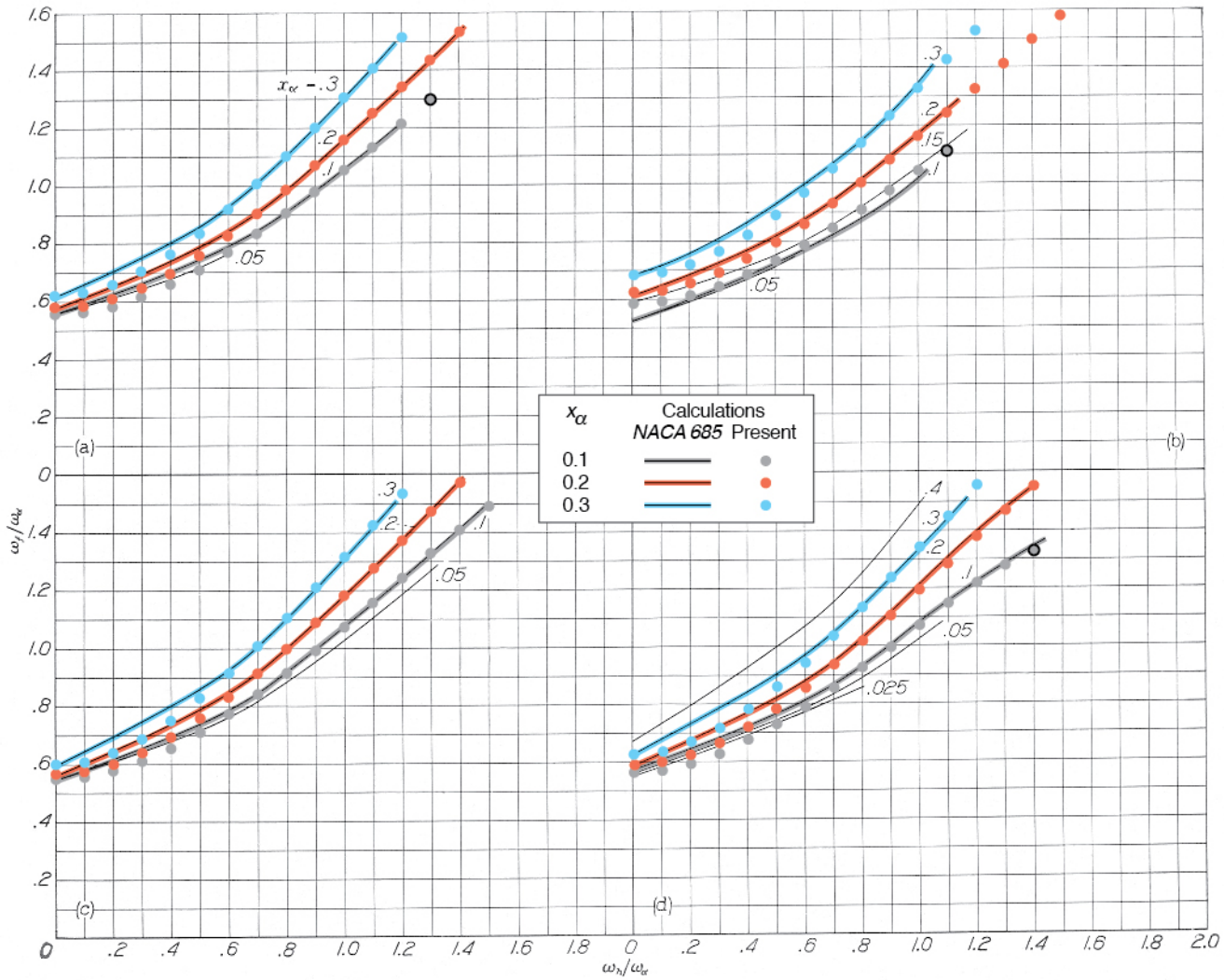

(a) $\kappa=\frac{1}{5}$; $a=-0.4$.
(c) $\kappa=\frac{1}{10}$; $a=-0.4$.

(b) $\kappa=\frac{1}{5}$; $a=-0.2$.
(d) $\kappa=\frac{1}{10}$; $a=-0.2$.

Graph I–F (a–d).—Flutter frequency ratio as dependent on x_α against frequency ratio; $r_\alpha{}^2=\frac{1}{4}$. Case 1 (h, α).

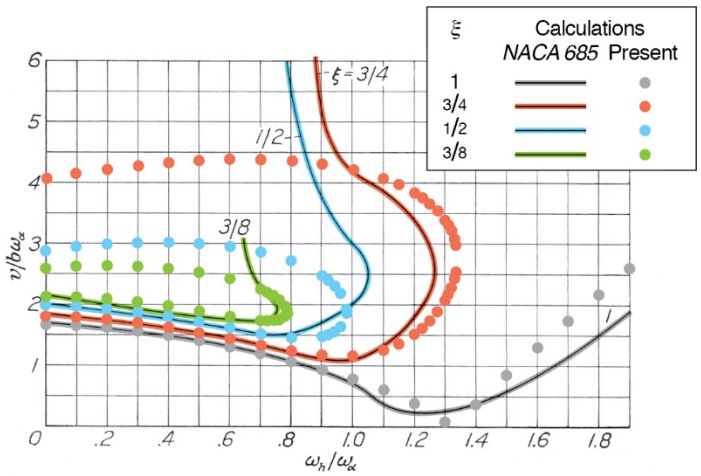

Graph I–G.—The effect of the coupling factor ξ; the flutter coefficient against the frequency ratio; $\kappa=\frac{1}{10}$; $a=-0.2$; $x_\alpha=0.2$.

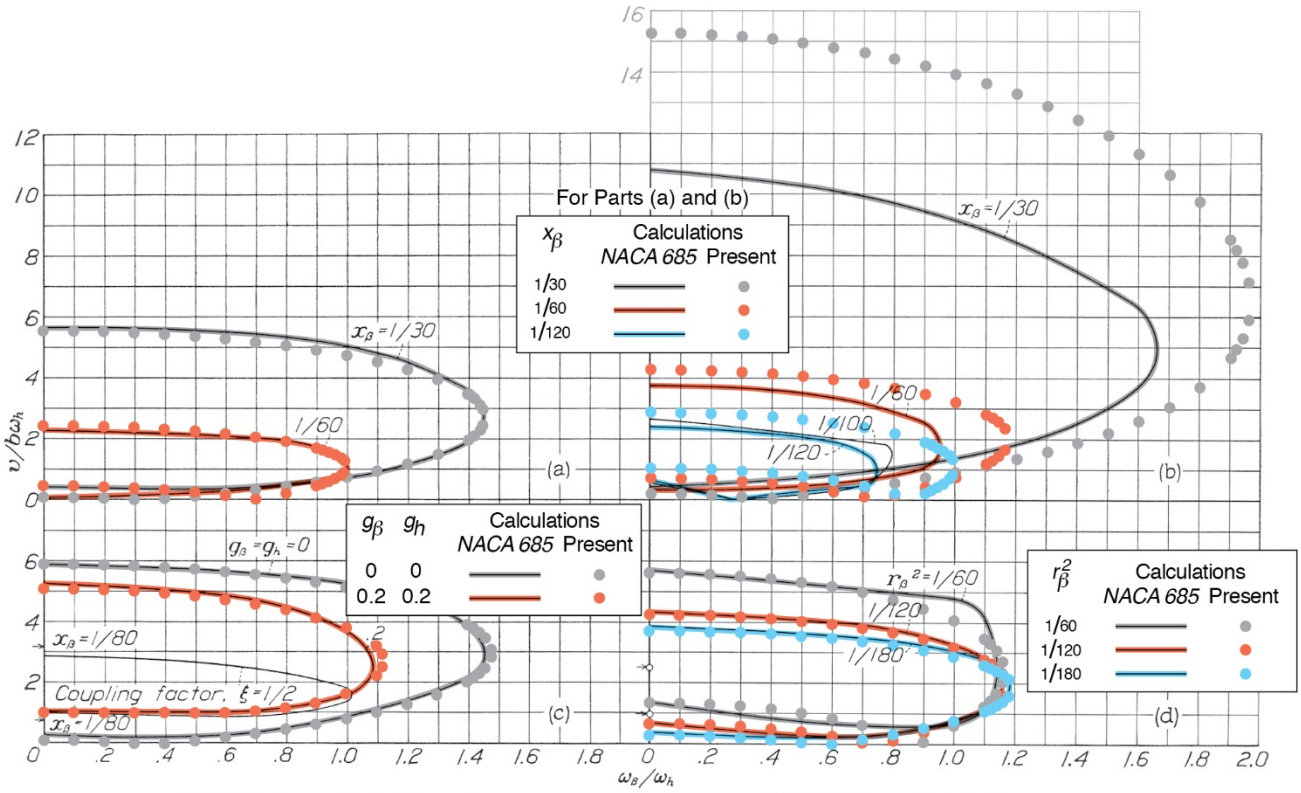

(a) Effect of x_β; $\kappa=\frac{1}{5}$; $r_\beta^2=\frac{1}{120}$.
(b) Effect of x_β; $\kappa=\frac{1}{10}$; $r_\beta^2=\frac{1}{120}$.
(c) Effect of g_β and g_h; $\kappa=\frac{1}{10}$; $r_\beta^2=\frac{1}{160}$; $x_\beta=\frac{1}{40}$.
(d) Effect of r_β^2; $\kappa=\frac{1}{10}$; $x_\beta=\frac{1}{60}$.

Graph II–A (a–d).—Flutter coefficient against frequency ratio; $c=\frac{1}{2}$. Case 2 (β, h).

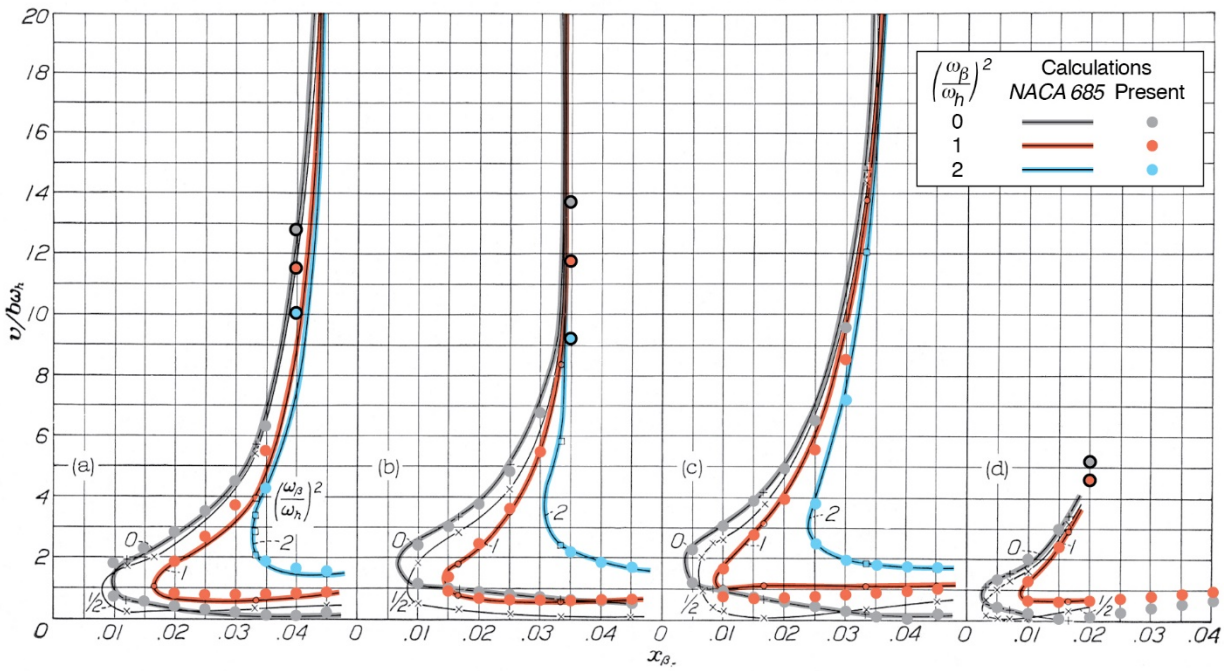

(a) $c=\frac{1}{2}$; $\kappa=\frac{1}{5}$; $r_\beta^2=\frac{1}{120}$.
(b) $c=\frac{1}{2}$; $\kappa=\frac{1}{5}$; $r_\beta^2=\frac{1}{60}$.
(c) $c=\frac{1}{2}$; $\kappa=\frac{1}{10}$; $r_\beta^2=\frac{1}{120}$.
(d) $c=\frac{2}{3}$; $\kappa=\frac{1}{5}$; $r_\beta^2=\frac{1}{500}$.

Graph II–B (a–d).—Flutter coefficient against x_β for various frequency ratios. Case 2 (β, h).

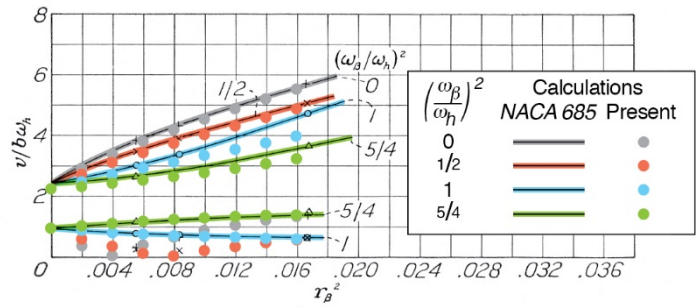

Graph II–C.—Flutter coefficient against r_β^2 for various frequency ratios; $c=\frac{1}{2}$; $\kappa=\frac{1}{10}$; $x_\beta=\frac{1}{60}$. Case 2 (β, h).

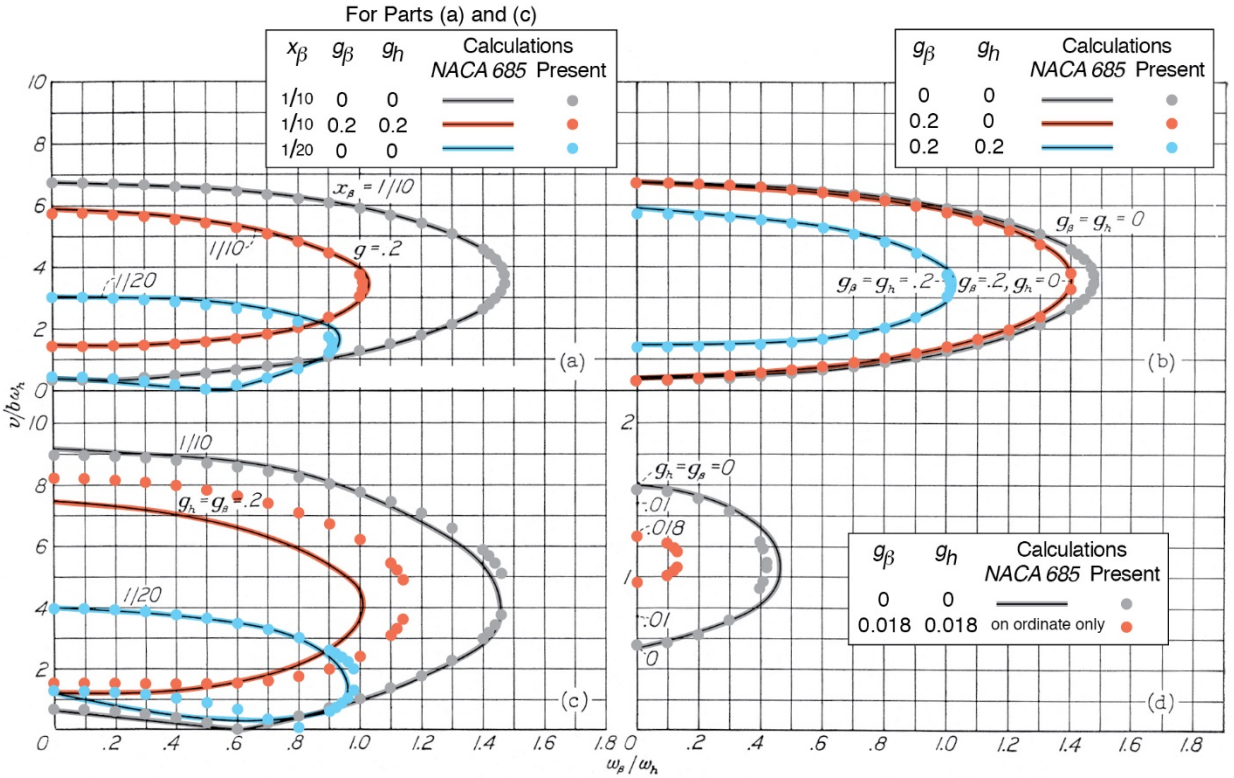

(a) $\kappa=\frac{1}{5}$; $r_\beta^2=\frac{1}{20}$; $x_\beta=\frac{1}{10}$, $\frac{1}{20}$.
(b) $\kappa=\frac{1}{5}$; $r_\beta^2=\frac{1}{20}$; $x_\beta=\frac{1}{10}$.
(c) $\kappa=\frac{1}{5}$; $r_\beta^2=\frac{1}{10}$; $x_\beta=\frac{1}{10}$, $\frac{1}{20}$.
(d) $\kappa=\frac{1}{5}$; $r_\beta^2=\frac{1}{20}$.

Graph II–D (a–d).—Flutter coefficient against frequency ratio, showing effect of x_β, g_β, and g_h; $c=0$. Case 2 (β, h).

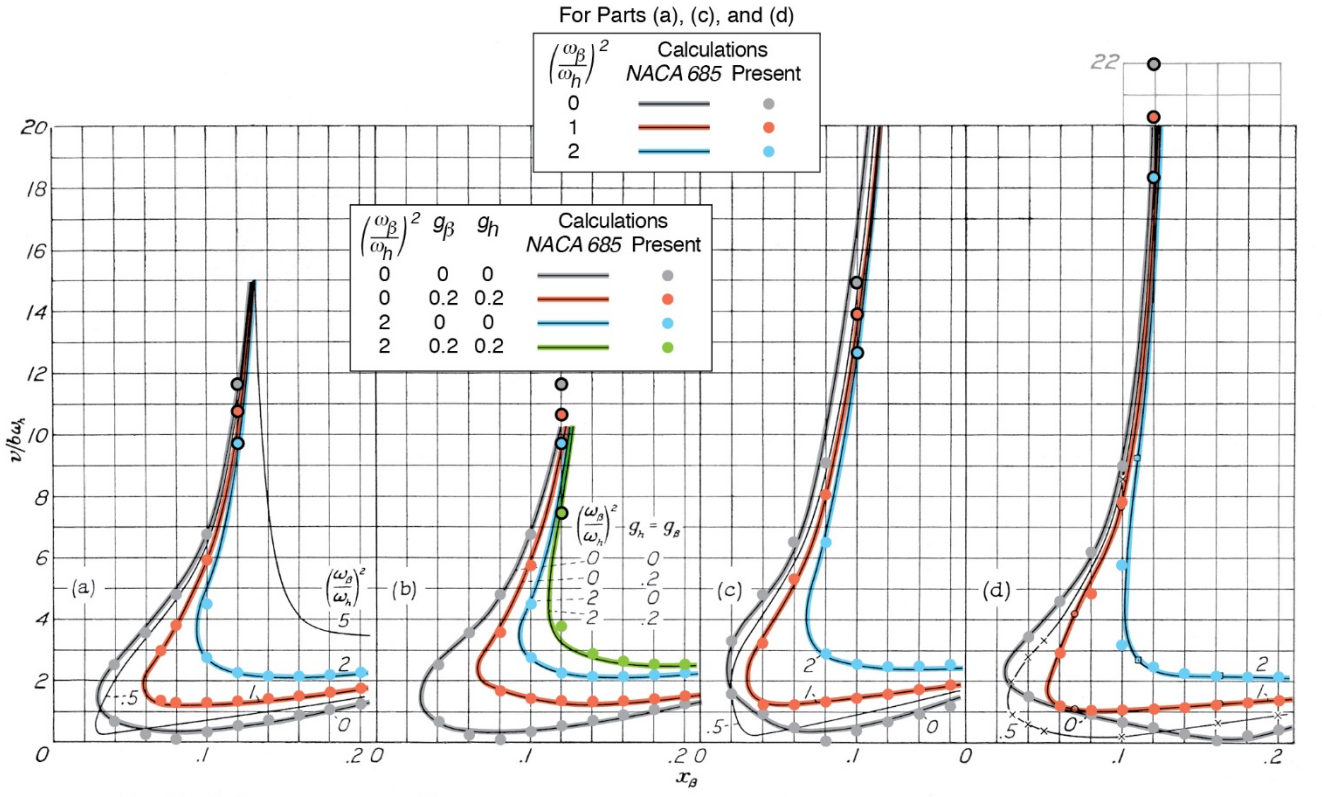

(a) $\kappa=\frac{1}{5}$; $r_\beta^2=\frac{1}{20}$. (b) $\kappa=\frac{1}{5}$; $r_\beta^2=\frac{1}{20}$. (c) $\kappa=\frac{1}{10}$; $r_\beta^2=\frac{1}{20}$. (d) $\kappa=\frac{1}{5}$; $r_\beta^2=\frac{1}{10}$.

Graph II–E (a–d).—Flutter coefficient against x_β for various frequency ratios; $c=0$. Case 2 (β, h).

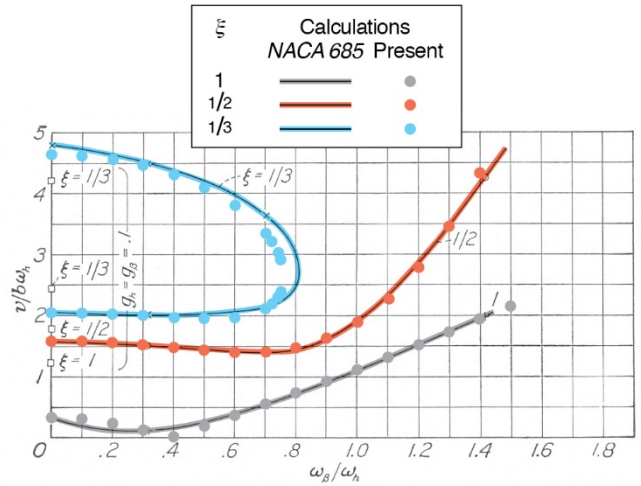

Graph II–F.—Effect of coupling factor ξ; flutter coefficient against frequency ratio; $c=0$; $\kappa=\frac{1}{5}$; $r_\beta^2=\frac{1}{6}$; $x_\beta=\frac{1}{4}$ (an extreme case of unbalance). Also effect of friction for $\omega_\beta/\omega_h=0$.

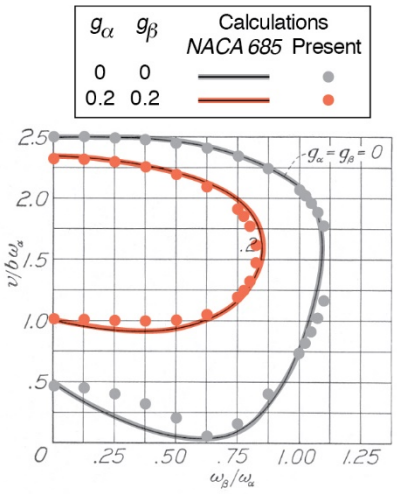

Graph III–A.—Effect of friction coefficients g_α, g_β; flutter coefficient against frequency ratio; c=0.5; κ=1/10; a=−0.4; r_α^2=1/4; x_β=1/80; r_β^2=1/160. Case 3.

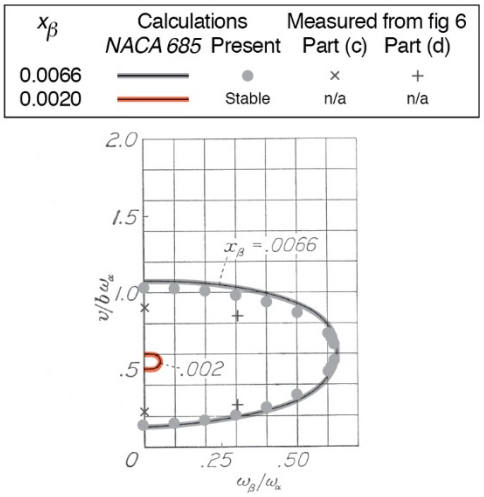

Graph III–B.—Effect of x_β; flutter coefficient against frequency ratio; c=0.6; κ=1/4; a=−0.4; r_α^2=1/4; r_β^2=0.0012. Case 3(α, β).

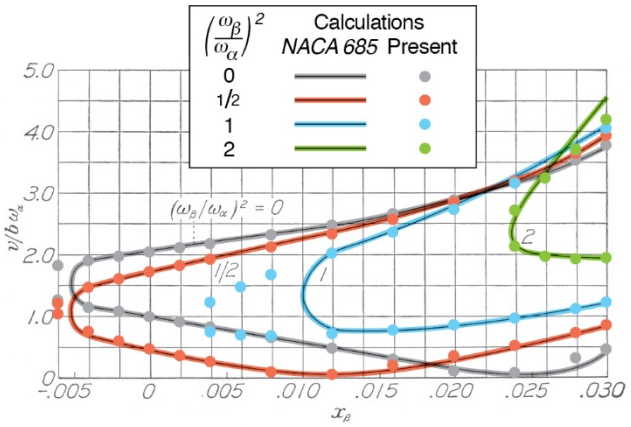

Graph III–C.—Flutter coefficient against x_β for various frequency ratios. c=0.5; κ=1/10; r_α^2=1/4; r_β^2=1/160; a=−0.4. Case 3.

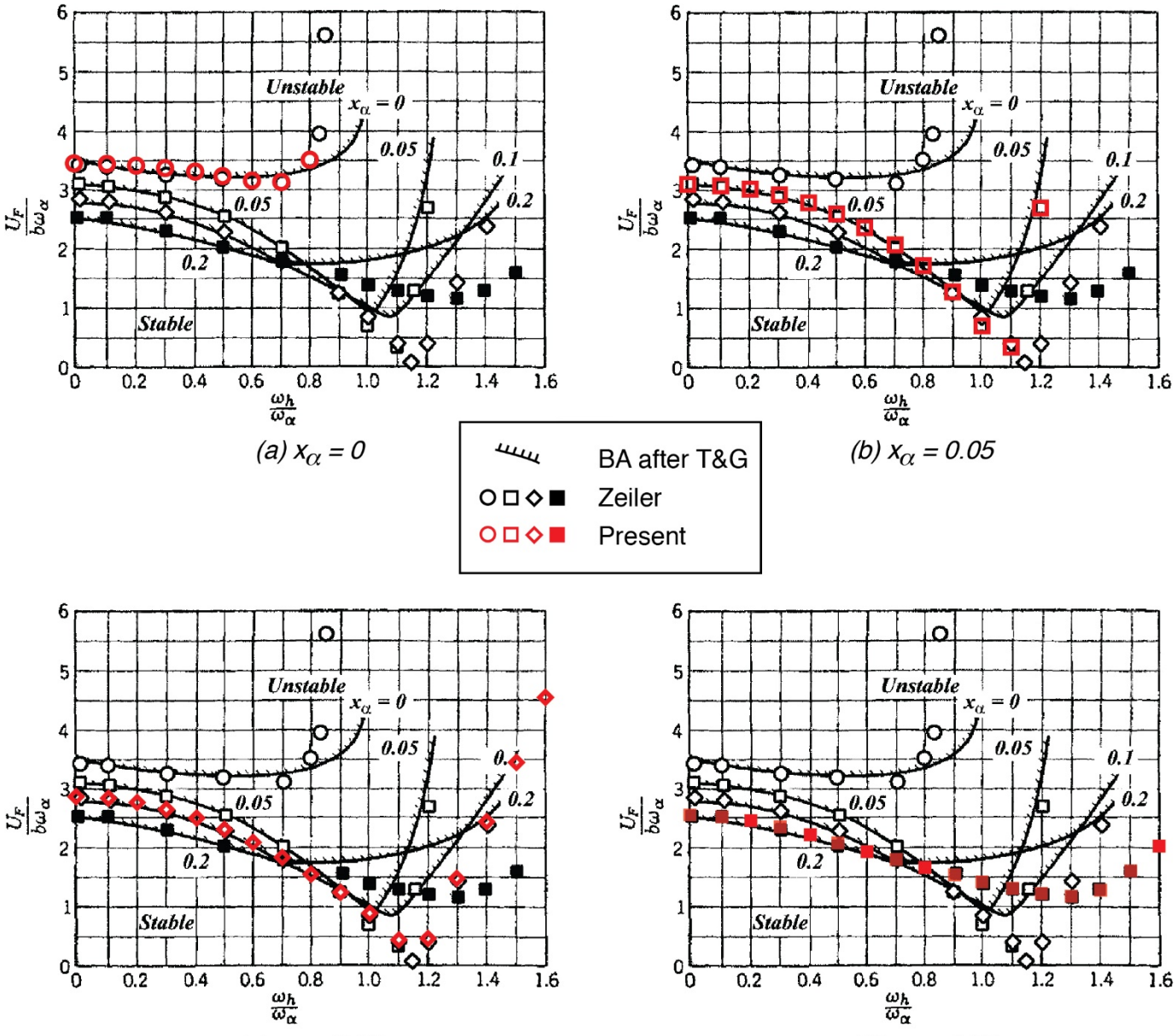

Figure B1. – Comparison of present recomputations with Zeiler's recomputations (from fig. 2 of ref. 1).

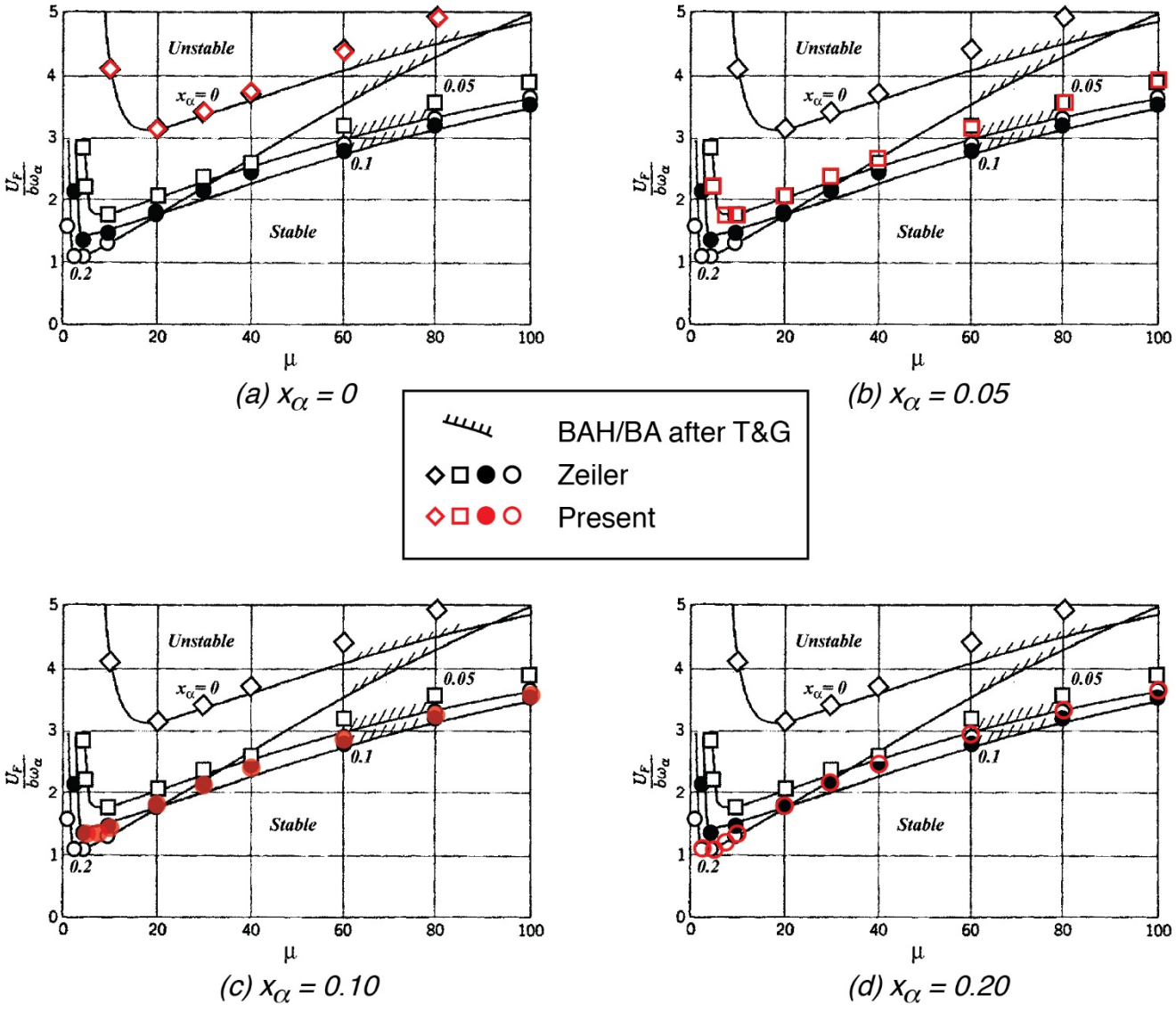

Figure B2. – Comparison of present recomputations with Zeiler's recomputations (from fig. 3 of ref. 1).

REPORT DOCUMENTATION PAGE

Form Approved
OMB No. 0704-0188

1. REPORT DATE *(DD-MM-YYYY)*	2. REPORT TYPE	3. DATES COVERED *(From - To)*
01-02- 2020	Technical Publication	

4. TITLE AND SUBTITLE

Re-Computation of Numerical Results Contained in NACA Report No. 685

5a. CONTRACT NUMBER

5b. GRANT NUMBER

5c. PROGRAM ELEMENT NUMBER

6. AUTHOR(S)

Perry, Boyd, III

5d. PROJECT NUMBER

5e. TASK NUMBER

5f. WORK UNIT NUMBER

432938.11.01.07.43.40.08

7. PERFORMING ORGANIZATION NAME(S) AND ADDRESS(ES)

NASA Langley Research Center
Hampton, VA 23681-2199

8. PERFORMING ORGANIZATION REPORT NUMBER

L-21099

9. SPONSORING/MONITORING AGENCY NAME(S) AND ADDRESS(ES)

National Aeronautics and Space Administration
Washington, DC 20546-0001

10. SPONSOR/MONITOR'S ACRONYM(S)

NASA

11. SPONSOR/MONITOR'S REPORT NUMBER(S)

NASA/TP-2020-220562

12. DISTRIBUTION/AVAILABILITY STATEMENT

Unclassified - Unlimited
Subject Category 01
Availability: STI Program (757) 864-9658

13. SUPPLEMENTARY NOTES

14. ABSTRACT In an engineering note published in the Journal of Aircraft in the year 2000, Thomas A. Zeiler made generally known that some of the early works on aeroelastic flutter by Theodore Theodorsen and I.E. Garrick (NACA Report Nos. 496, 685, and 741) contained numerical errors in some of their numerical examples. Some of the plots containing numerical errors were later reproduced in two classic aeroelasticity texts (BAH and BA). Because these foundational papers and texts are often used in graduate courses on aeroelasticity, Zeiler recommended that an effort be undertaken to employ the computational resources available today (digital computers) to recompute the example problems in these early works and to publish the results so as to provide a complete and error-free set of numerical examples. This paper presents recomputed theoretical results contained in NACA Report No. 685 (NACA 685), "Mechanism of Flutter, A Theoretical and Experimental Investigation of the Flutter Problem," by Theodore Theodorsen and I.E. Garrick. The recomputations were performed employing the solution method described in NACA 685, but using modern computational tools. With some exceptions, the magnitudes and trends of the original results were in good-to-excellent agreement with the recomputed results, a surprising but gratifying result considering that the NACA 685 results were computed "by hand" using pencil, paper, slide rules, and mechanical calculators called comptometers. Checks on the recomputations (about 25% were checked) were performed using the so-called p-method of flutter solution. In all cases, including those where the original and recomputed results differed significantly, the checks were in excellent agreement with the recomputed results.

15. SUBJECT TERMS

Aeroelastic stability; Flutter; NACA Report No. 685; Theodore Theodorsen; I.E. Garrick

16. SECURITY CLASSIFICATION OF:			17. LIMITATION OF ABSTRACT	18. NUMBER OF PAGES	19a. NAME OF RESPONSIBLE PERSON
a. REPORT	b. ABSTRACT	c. THIS PAGE			STI Help Desk (email: help@sti.nasa.gov)
					19b. TELEPHONE NUMBER *(Include area code)*
U	U	U	UU	73	(757) 864-9658